Revista Brasiliense de Engenharia e Física Aplicada
Vol. 10 Nº 1 – Julho/Agosto 2025

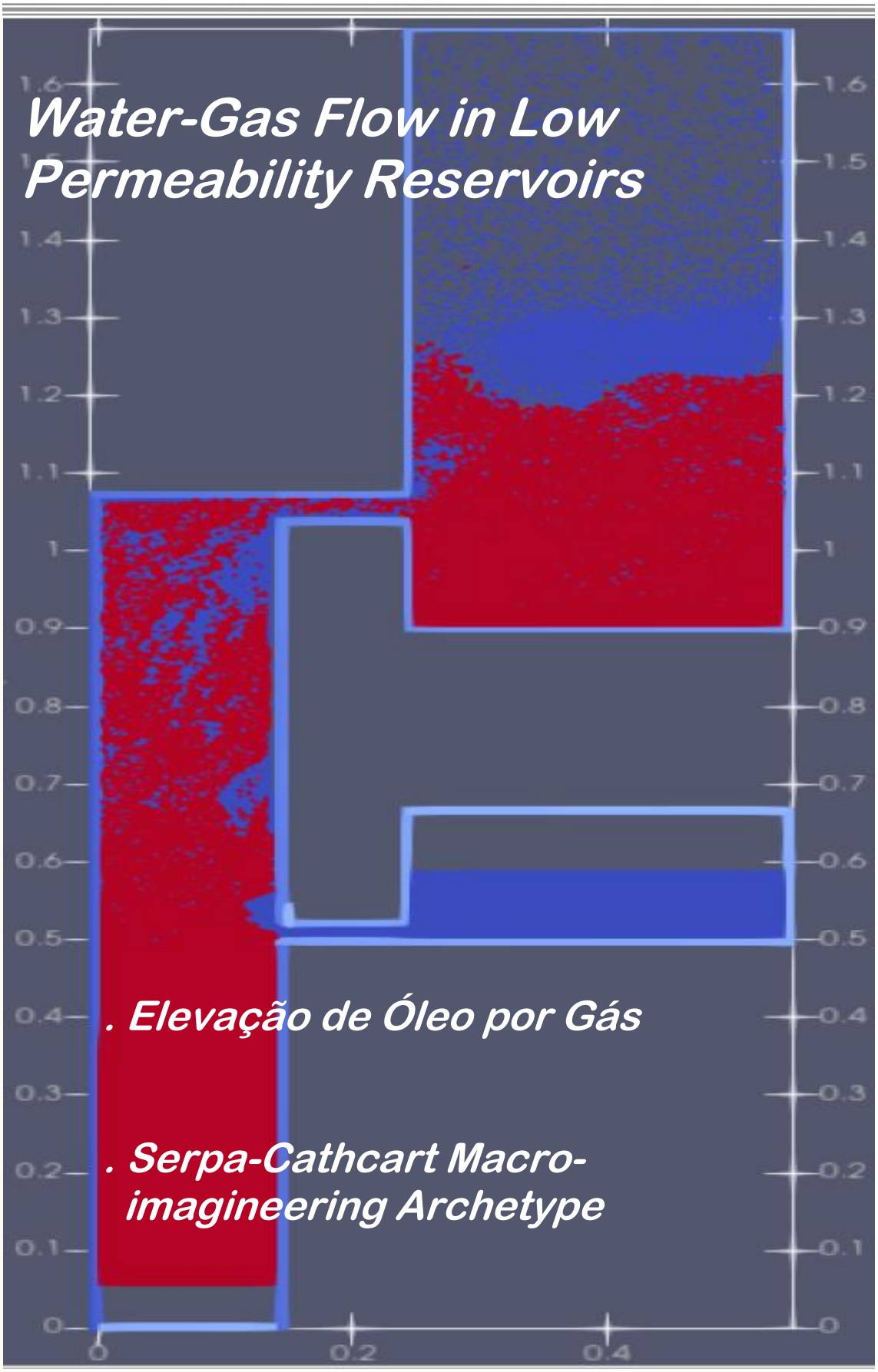

ISSN 2526-4192

ÍNDICE

ARTIGOS ORIGINAIS

Simulação da Elevação de Óleo por Gás usando o Método Smoothed Particle Hydrodynamics

Naim Jesse dos Santos Carvalho

Pós-graduação em Modelagem Computacional, Instituto Politécnico, Universidade do Estado do Rio de Janeiro, Brasil.

Livia Flavia Carletti Jatobá

Departamento de Engenharia Mecânica e Energia, Instituto Politécnico, Universidade do Estado do Rio de Janeiro, Brasil.

Grazione de Souza

Departamento de Modelagem Computacional, Instituto Politécnico, Universidade do Estado do Rio de Janeiro, Brasil.

Helio Pedro Amaral Souto

Departamento de Modelagem Computacional, Instituto Politécnico, Universidade do Estado do Rio de Janeiro, Brasil.

Abstract: Oil reservoir production typically declines over time due to decreasing pressure, posing a challenge to maintaining economically viable production rates. To supplement natural flow, artificial lift methods can be employed to enhance fluid recovery. The choice of a suitable lift method depends on the characteristics of the production system, including reservoir and fluid properties, as well as surface facility constraints. This study focuses on gas lift, an artificial lift technique that involves injecting compressed gas into the lower sections of the well through valves strategically placed along the production tubing. As the injected gas mixes with the oil, it reduces the effective density of the fluid mixture, thereby facilitating its ascent to the surface. Gas lift is particularly well suited for offshore operations and is not constrained by well depth. It allows for either continuous or intermittent lifting to restore or enhance productivity. Despite its relevance, numerical simulations of gas lift rarely employ particle-based methods. One such method is Smoothed Particle Hydrodynamics (SPH), which is a mesh free Lagrangian approach capable of modeling multiphase flows. In this work, we apply the SPH method to a simplified gas lift test case: a two-dimensional, two-phase isothermal flow in a vertical pipe filled with oil, into which high-pressure gas is injected through a valve. Our simulation results demonstrate the feasibility of using SPH to model gas lift. However, further refinement of the boundary conditions is required for the method to become truly competitive.

Palavras-chave: artificial lift, gas-lift, oil production, Smoothed Particle Hydrodynamics.

Corresponding author: Helio Pedro Amaral Souto, helio@iprj.uerj.br

Received: 26 May 2025 / Accepted: 04 Jun 2025 / Published: 11 Aug 2025.

1 Introdução

Para maximizar a produção de óleo e gás, a engenharia tem buscado desenvolver técnicas que exigem o conhecimento da dinâmica do escoamento dos fluidos nos reservatórios e dutos. A compreensão do escoamento multifásico é crucial em diversas dessas técnicas, como no estudo da elevação artificial empregando o método gas lift [13].

Embora um reservatório possa, inicialmente, apresentar energia suficiente para elevar os fluidos da formação até a superfície, com o passar do tempo a energia no sistema diminui, podendo atingir um ponto em que a vazão dos poços se torna economicamente inviável para a sua produção [20].

Portanto, as técnicas de elevação artificial no transporte de hidrocarbonetos em dutos são ferramentas empregadas para evitar a queda da vazão, garantindo o escoamento do óleo do reservatório até a superfície, uma vez que fornecem uma energia adicional ao fluido presente na coluna de produção. Dentre as técnicas comumente utilizadas, encontram-se: o bombeio centrífugo submerso, o bombeio por cavidades progressivas, o bombeio mecânico e o gas lift contínuo e intermitente [24].

A técnica de gas lift, portanto, visa a aumentar a produção por meio da gaseificação da coluna de produção. Conforme o gás é injetado, sua expansão e consequente combinação com o fluido residente resultam em uma mistura com menor densidade efetiva. Assim, ela é mais facilmente transportada até a superfície [3].

Na modalidade intermitente, o gas lift consiste na injeção de gás na coluna de produção em intervalos de tempo e volumes predeterminados por ciclo. Um ciclo, conforme definido por Clodoaldo [5], compreende as seguintes etapas:

1. Injeção: o gás a alta pressão é injetado por um certo período;
2. Elevação: a carga de líquido é carregada para a superfície em função do surgimento do escoamento em golfada;
3. Produção: a golfada atinge o topo (a superfície) e o fluido, então, é escoado para a linha de produção;
4. Descompressão: a coluna é descomprimida conforme o gás presente no seu interior é levado à superfície;
5. Alimentação: ocorre a restauração da carga de líquido na coluna principal de escoamento.

Na elevação contínua, o gás é injetado ininterruptamente no duto, mantendo uma pressão suficientemente baixa em relação à pressão do reservatório, permitindo que seja alcançada a vazão almejada [21]. Em geral, gás natural é utilizado em ambas as modalidades, sendo composto por uma mistura de hidrocarbonetos de baixa massa molecular, como o metano e o etano (seus principais componentes), em estado gasoso. Também podem estar presentes outros compostos, como o nitrogênio e "impurezas", tais como o dióxido de carbono (CO_2) e o sulfeto de hidrogênio (H_2S) [13].

Diversos estudos que tratam da elevação artificial usando o gas lift podem ser encontrados na literatura. No entanto, o número de trabalhos utilizando códigos livres e abertos em sua simulação numérica ainda é reduzido. Dentre alguns trabalhos recentes, citamos aqueles que empregam abordagens experimentais e numéricas. Iniciamos com o de Guerra et al. [12], que realizaram estudos experimentais em sistemas água-ar. Eles analisaram os efeitos da variação do ângulo de injeção do gás na queda de pressão do sistema e focaram na obtenção de dados relativos ao diâmetro e à forma das bolhas, ângulos de deflexão do jato de ar e perfis de velocidade médios.

Em outro artigo, Abdulkadir et al. [1] realizaram experimentos em um duto vertical, considerando os regimes de escoamento do tipo golfadas (slug flow), onde a fase gasosa era o ar e a líquida, o óleo de silicone. O objetivo era comparar o comportamento das fases com os resultados obtidos em simulações numéricas, utilizando os softwares Star-CD e Star-CCM+, para a determinação da fração de fase.

Por sua vez, Sami e Turzo [21] caracterizaram alguns escoamentos, em regime intermitente, bifásicos óleo-gás, utilizando o software Fluent (Ansys 19). Os autores buscaram verificar se o modelo utilizado no simulador era capaz de predizer a velocidade no escoamento em golfadas para diferentes pressões de injeção. Eles chegaram à conclusão de que o aumento da pressão levava ao incremento da velocidade inicial da golfada, próximo à região de injeção, com posterior diminuição até atingir a superfície.

Utilizando o Computational Fluid Dynamics (CFD) Fluent 18.5, Hussein et al. [14] simularam o escoamento água-ar. Nesse estudo, a fase gasosa era injetada no fundo de um duto vertical, enquanto a água era injetada pelas laterais. O objetivo era avaliar a ocorrência do escoamento anular, no qual um anel composto por um dos fluidos se forma na tubulação. Foi calculado o campo de velocidades no escoamento e determinada a velocidade crítica do gás.

O software STAR-CCM+ CFD foi empregado por Parsi et al. [19] para estudar os regimes de escoamento em golfadas e o churn flow, confrontando os resultados numéricos da distribuição da fração de fase com aqueles obtidos em experimentos. Eles constataram boa concordância entre ambas as abordagens, à medida que o tempo evoluía, para a distribuição espacial das fases.

Tocci, Bos e Henkes [25] propuseram a adoção de um modelo híbrido que combina o método Volume of Fluid (VOF) [7] e um modelo multi-fluido. Inicialmente, os autores utilizaram o OpenFOAM para simular um escoamento água-ar em um duto vertical, no qual o líquido entrava no domínio pela extremidade inferior, formando um filme (ou "anel"), enquanto o gás era injetado, na mesma localização, pela seção central. Eles verificaram que a distribuição da fração de fase se assemelhava àquelas reportadas por outros autores usando o software Fluent. No entanto, a divergência encontrada em relação aos resultados experimentais para a mesma configuração levou os autores a proporem o modelo híbrido: o VOF seria utilizado para a detecção e representação das regiões de separação entre as fases, enquanto o modelo multi-fluido seria empregado na simulação das regiões com presença de bolhas de gás dispersas no fluido.

Um estudo com proposição semelhante (modelo híbrido) foi realizado por Wardle e Weller [27], que também utilizaram o OpenFOAM na simulação de escoamentos segregados e dispersos. Entretanto, eles objetivaram simular sistemas de extração líquido-líquido, nos quais o ar era a terceira fase presente.

Douillet-Grellier et al. [9] usaram uma implementação do método Smoothed Particle Hydrodynamics (SPH) na simulação de escoamentos bifásicos óleo-gás bidimensionais em dutos. Os autores buscavam confirmar a reprodutibilidade dos regimes de escoamento previstos por Taitel e Dukler [23] e, então, identificaram os processos de transição entre os regimes. No entanto, limitaram-se à simulação de escoamentos em dutos horizontais ou inclinados, não abordando instalações com dutos verti-

cais. Problemas similares também já foram abordados via método SPH em Carvalho [4, 8].

Diante do exposto, o presente trabalho visa a verificar a viabilidade da utilização da versão multifásica do DualSPHysics [6] no estudo da técnica de gas lift. Realizamos um estudo inicial com o objetivo de simular a injeção de gás em um circuito contendo um trecho do duto de transporte e um reservatório para separação da mistura gás-óleo.

2 Equações Governantes

Da Mecânica do Contínuo, sabemos que as equações da continuidade e de Navier-Stokes governam o escoamento de fluidos newtonianos compressíveis. Aqui, apresentamos essas equações em suas respectivas representações lagrangianas.

A equação da continuidade, que expressa a conservação da massa, é dada na forma [16]:

$$\frac{D\rho}{Dt} + \rho\nabla\cdot\vec{v} = 0, \tag{1}$$

onde ela é escrita em termos da derivada material (D/Dt), ρ é a massa específica, t é o tempo e $\vec{v}$ representa o vetor velocidade.

Por outro lado, da conservação da quantidade de movimento obtemos a equação de Navier-Stokes (válida para fluidos newtonianos) [16]:

$$\rho\frac{D\vec{v}}{Dt} = -\nabla P + \mu\nabla^2\vec{v} - \frac{2}{3}\nabla\left(\mu\nabla\cdot\vec{v}\right) + \vec{f_e}, \tag{2}$$

onde P representa a pressão termodinâmica, μ é a viscosidade do fluido e $\vec{f_e}$ é o vetor relativo às forças externas.

Como vamos considerar somente o escoamento isotérmico, não precisaremos resolver a equação da energia e, portanto, ela não é apresentada. Em se tratando do escoamento não isotérmico, os leitores podem encontrá-la em [16], incluindo a sua versão discretizada.

Em simulações utilizando o método SPH, uma abordagem possível para a simulação do escoamento de fluidos incompressíveis envolve a hipótese de considerá-lo como sendo ligeiramente compressível [10]. Portanto, a equação de estado de Tait é frequentemente utilizada para a determinação da pressão, como uma função da massa específica. Comumente utilizada na simulação de escoamentos com superfícies livres, ela possui versões que descrevem acuradamente fenômenos tais como a propagação de ondas sonoras na água [2].

Aqui, adotamos como equação de estado [17]:

$$P(\rho) = \frac{c_s^2\rho_0}{\gamma}\left[\left(\frac{\rho}{\rho_0}\right)^{\gamma} - 1\right] + P_f - a\rho^2, \tag{3}$$

onde γ é o fator de expansão isentrópica (relação entre os calores específicos a pressão e volume constantes), ρ_0 é a massa específica inicial do fluido, c_s é a velocidade do som, P_f é a pressão de fundo (definida pelo usuário ou calculada a partir da configuração inicial do problema) e o último termo introduz as forças coesivas que atuam entre as partículas de uma dada fase. O coeficiente a é determinado com base nas propriedades das fases e no comprimento característico do problema, L_c [8]

$$a = 1,5g\left(\frac{\rho_\alpha}{\rho_\beta}\right)L_c, \tag{4}$$

onde g é a magnitude da aceleração devido à gravidade, e ρ_α e ρ_β são as massas específicas iniciais das duas fases presentes no escoamento. O comprimento característico é uma constante empírica que depende das dimensões do domínio e da distância inicial entre as partículas [8].

3 Metodologia Numérica

Usando as "Aproximações Integral e de Partículas" [8, 16] e tomando $v_{ij} = v_i - v_j$, as formas discretizadas das Equações Governantes (1) e (2) podem ser obtidas no formalismo do método SPH.

Inicialmente, apresentamos a forma discretizada da equação de continuidade [16]:

$$\frac{D\rho_i}{Dt} = \sum_{j=1}^{N} m_j v_{ij}\cdot\nabla_i W_{ij}^h, \tag{5}$$

sendo que m_j representa a massa da partícula j, $W_{ij}^h = W(r_{ij}, h)$, W é a função núcleo (ou kernel), $r_{ij} = |x_i - x_j|$, h é o comprimento de suavização, e o gradiente da função núcleo é determinado em relação à partícula i, tal que:

$$\nabla_i W_{ij}^h = \frac{x_{ij}}{r_{ij}}\frac{\partial W_{ij}^h}{\partial r_{ij}}, \tag{6}$$

onde x_{ij} representa a distância entre duas partículas i e j ($x_{ij} = x_i - x_j$).

Todas as simulações foram realizadas usando uma função kernel do tipo spline quintic [28]:

$$W(r,h) = \alpha_d\left(1 - \frac{q}{2}\right)^4(2q+1) \qquad 0 \le q \le 2, \tag{7}$$

onde $q = r/h$ representa a distância (r) adimensionalizada entre as partículas, $\alpha_d = 3/4h$, $7/(4\pi h^2)$ e $21/(16\pi h^3$ para problemas uni, bi e tridimensionais, respectivamente.

Devido à presença da fase gasosa e às descontinuidades na interface de separação das fases, a formulação tradicional usada no método SPH não é mais aplicável. Então, um termo extra é adicionado à equação do momentum (o quarto termo do lado direito do sinal da igualdade) para levarmos em conta as forças coesivas da fase menos densa [22]:

$$\frac{D\vec{v}_i}{Dt} = -\sum m_j\left(\frac{P_i + P_j}{\rho_i\rho_j}\right)\nabla_i W_{ij} + \sum_j m_j\left[\frac{4\mu r_{ij}\cdot\nabla_i W_{ij}}{(\rho_i+\rho_j)\left(r_{ij}^2+\eta^2\right)}\right]$$

$$+\sum_j m_j\left(\frac{\tau_{ij}^j}{\rho_j^2}+\frac{\tau_{ij}^i}{\rho_i^2}\right)\nabla_i W_{ij}$$
$$\underbrace{-2a\rho_\alpha^2\sum_j\frac{m_j}{\rho_j}\nabla_i W_{ij}}_{\text{para a fase gasosa}}+\vec{F}_s+\vec{g}, \tag{8}$$

onde os efeitos da tensão viscosa foram decompostos em dois termos: uma contribuição devida à tensão viscosa laminar e outra à tensão viscosa na Escala da Subpartícula (Sub-Particle Scale, SPS), tendo o conceito sido proposto por Gotoh, Shibahara e Sakai [11], de modo a introduzir os efeitos da turbulência no modelo Moving Particle Semi-implicit (MPS), e τ_{ij} representa os componentes do tensor de tensão da subpartícula:

$$\frac{\tau_{ij}}{\rho}=\nu_t\left(2S_{ij}-\frac{2}{3}k\delta_{ij}\right)-\frac{2}{3}C_I\Delta l^2\delta_{ij}|S_{ij}|^2, \tag{9}$$

onde $\nu_t=(C_S\Delta l)^2\sqrt{2S_{ij}S_{ij}}$ é a viscosidade turbulenta, C_S a constante de Smagorinsky, Δl representa a distância inicial entre as partículas, k a energia cinética de turbulência do modelo SPS, C_I um parâmetro constante, δ_{ij} é o delta de Kronecker, S_{ij} os componentes do tensor taxa de deformação do modelo SPS, e η é um número pequeno introduzido para evitarmos a divisão por zero e geralmente é considerado como sendo igual a $0{,}1h$.

A força superficial, por unidade de área, geralmente é expressa a partir do método da Tensão Superficial Contínua [8], que utiliza a curvatura da interface de separação das fases, κ, de modo que:

$$\vec{F}_s=\kappa\sigma_\alpha\vec{n} \tag{10}$$

onde σ_α é a tensão superficial da fase α e $\vec{n}$ é o vetor normal unitário à superfície. O cálculo da curvatura pode não ser uma tarefa fácil. Destarte, na literatura foi proposta a sua determinação via o tensor de pressão capilar $\mathbf{\Pi}$ [9, 15]:

$$\vec{F}_s=-\nabla\cdot\mathbf{\Pi}, \tag{11}$$

sendo que o tensor é dado por [8]:

$$\mathbf{\Pi}=-\sigma\left(\mathbf{I}-\hat{n}\otimes\hat{n}\right)|\nabla C|, \tag{12}$$

onde C é a função cor definida, para uma partícula i pertencente à fase α, como:

$$C_i^\alpha=\begin{cases}1 & \text{se } i\in\alpha,\\ 0 & \text{se } i\notin\alpha.\end{cases} \tag{13}$$

Essa função representa um salto unitário na interface e a normal unitária, presente na Equação (12), pode ser determinada na forma:

$$\hat{n}=\frac{\nabla C}{|\nabla C|}. \tag{14}$$

No presente modelo, a força devida à tensão superficial, Equação (8), é computada como sendo uma força externa [8]:

$$\vec{F}_s=\sum_j m_j\frac{\Pi_i^{\alpha\beta}+\Pi_j^{\alpha\beta}}{\rho_i\rho_j}\frac{\partial W}{\partial r_{ij}}, \tag{15}$$

onde α e β representam as duas fases que interagem entre si e as componentes do tensor $\Pi_i^{\alpha\beta}$ são determinadas na forma [15]:

$$\Pi_i^{\alpha\beta}=\sigma^{\alpha\beta}\frac{1}{\left|\nabla C_i^{\alpha\beta}\right|}\left(\frac{1}{d}\left|\nabla C_i^{\alpha\beta}\right|^2\delta^{\alpha\beta}\right)$$
$$-\sigma^{\alpha\beta}\frac{1}{\left|\nabla C_i^{\alpha\beta}\right|}\left(\nabla C_i^{\alpha\beta}\otimes\nabla C_i^{\alpha\beta}\right), \tag{16}$$

na qual d é o número de dimensões do problema (1, 2 or 3) e o gradiente da função cor, para uma partícula i, pode ser calculado no formalismo do método SPH por [6]:

$$\nabla C_i^{\alpha\beta}=\sum_j\frac{m_j}{\rho_j}\left(C_j^\beta-C_i^\beta\right)\frac{\partial W}{\partial r_{ij}}. \tag{17}$$

4 Resolução do Sistema de Equações Diferenciais Ordinárias

Após a discretização das equações governantes do escoamento, nos deparamos com o sistema de equações diferenciais ordinárias:

$$\frac{D\vec{v}_i}{Dt}=\vec{F}_i, \tag{18}$$

$$\frac{D\rho_i}{Dt}=R_i, \tag{19}$$

$$\frac{D\vec{r}_i}{Dt}=\vec{v}_i, \tag{20}$$

onde a primeira equação representa, de forma simplificada, a equação do momentum, a segunda a da continuidade, e usamos a terceira para calcularmos o deslocamento das partículas de fluido.

Na resolução desse sistema, usamos o algoritmo de integração numérica de Verlet [26], geralmente utilizado em problemas da dinâmica molecular devido ao seu baixo custo computacional. Assim, quando o aplicamos na resolução do escoamento quase-compressível obtemos [4, 8]:

$$\vec{v}_i^{\,n+1}=\vec{v}_i^{\,n-1}+2\Delta t\vec{F}_i^{\,n}, \tag{21}$$

$$\vec{r}_i^{\,n+1}=\vec{r}_i^{\,n}+\Delta t\vec{v}_i^{\,n}+\frac{1}{2}\Delta t^2\vec{F}_i^{\,n}, \tag{22}$$

$$\rho_i^{n+1}=\rho_i^{n-1}+2\Delta t R_i^n, \tag{23}$$

onde o sobrescrito $n+1$ indica o próximo instante de tempo $t^{n+1}=t^n+\Delta t$.

Devido à natureza do método, desacoplamos no procedimento de cálculo os valores da massa específica e da velocidade no tempo $n+1$, pois eles não consideram os seus respectivos valores determinados no instante de tempo n (usando apenas a informação disponível em $n-1$). Tal fato pode levar à divergência do método numérico [6]. Assim, precisamos de um passo intermediário a cada N_s passos:

$$\vec{v}_i^{\,n+1} = \vec{v}_i^{\,n} + \Delta t \vec{F}_i^{\,n}, \tag{24}$$

$$\vec{r}_i^{\,n+1} = r_i^{\,n} + \Delta t \vec{v}_i^{\,n} + \frac{1}{2}\Delta t^2 \vec{F}_i^{\,n}, \tag{25}$$

$$\rho_i^{n+1} = \rho_i^n + 2\Delta t R_i^n. \tag{26}$$

Como usamos um método explícito, devemos impor restrições ao valor do incremento de tempo para garantir a sua estabilidade e convergência numéricas. Neste trabalho, determinamos o Δt de acordo com o proposto por Monaghan [18]:

$$\Delta t_f = min_i \left(\sqrt{\frac{h}{|f_i|}} \right), \tag{27}$$

$$\Delta t_{cv} = min_i \left(\frac{h}{c_s + max_j \left(\frac{h v_i \cdot r_i}{r_{ij}^2 + \eta^2} \right)} \right), \tag{28}$$

$$\Delta t = C_{CFL}\, min\left(\Delta t_f, \Delta t_{cv}\right), \tag{29}$$

sendo que Δt_f é calculado a partir da magnitude das forças por unidade de massa atuando na partícula i. Por outro lado, Δt_{cv} considera a estimativa da relação entre a distância percorrida pela partícula e a sua velocidade de deslocamento acrescida da do som. Nelas, h é o comprimento de suavização, v_i é a magnitude da velocidade da partícula i, c_s a velocidade do som e η foi introduzido a fim de evitarmos a divisão por zero. Resumindo, o valor do passo de tempo efetivamente empregado é determinado como sendo o valor mínimo entre Δt_f e Δt_{cv}, multiplicado pelo fator C_{CFL} pré-definido.

5 Resultados Numéricos

Como mencionado na introdução, realizamos simulações utilizando a versão multifásica do DualSPHysics [6] com o objetivo de estudar qualitativamente o fenômeno da elevação por gás (gas lift). Esse processo é amplamente utilizado na indústria petrolífera como método de recuperação artificial, sendo caracterizado pela injeção controlada de gás com o intuito de reduzir a densidade do fluido no duto de produção, facilitando, assim, o seu escoamento até a superfície.

Neste trabalho inicial, nosso foco esteve voltado para a modelagem conceitual e a definição adequada do domínio computacional. O sistema modelado inclui um duto principal por onde escoa o óleo, uma seção dedicada à injeção do gás e um reservatório posicionado no final do tubo, destinado à separação das fases. Tal configuração, embora simplificada, procura capturar os aspectos fundamentais do mecanismo de elevação por gás, permitindo a visualização dos efeitos da injeção contínua de gás sobre o padrão de escoamento e a eficiência da produção.

Cabe destacarmos que o problema-teste idealizado não representa diretamente um caso real. Entretanto, na concepção do modelo procuramos respeitar proporções fisicamente plausíveis, com base em dados da literatura técnica, no que diz respeito às razões entre os diâmetros dos tubos, às propriedades dos fluidos e às vazões de injeção tanto do óleo quanto do gás. Com isso, buscamos garantir a relevância prática dos resultados obtidos e oferecer uma base para estudos mais avançados com geometrias e condições operacionais mais complexas.

Ressaltamos que, em um trabalho anterior, o método SPH já havia sido aplicado com sucesso na identificação de padrões de escoamento durante a simulação de um escoamento multifásico de dois fluidos imiscíveis em dutos horizontais [4].

A Figura 1 apresenta uma representação esquemática do sistema, que consiste em um duto para o escoamento principal, uma seção de injeção de gás e um reservatório para a separação dos fluidos.

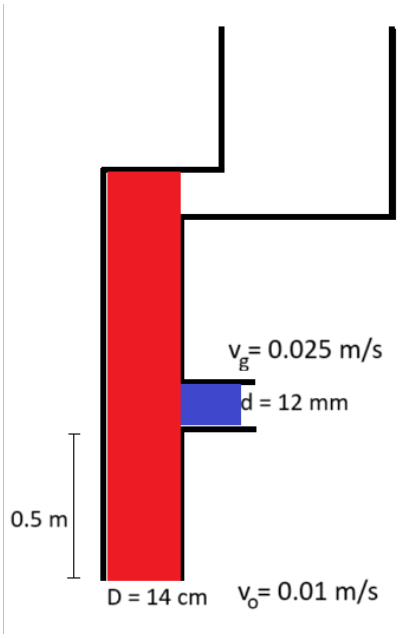

Figura 1: Representação do duto principal, de injeção e do reservatório de separação

De acordo com o que já dissemos, as dimensões do duto principal e da seção de injeção foram definidas em conformidade com os padrões industriais, sendo o diâmetro da injeção semelhante ao de uma válvula de controle em sistemas de gas lift. O reservatório de separação é necessário para que os efeitos da injeção de gás possam ser quantificados na recuperação do óleo.

Na Tabela 1, apresentamos os parâmetros usados em todas as simulações, enquanto as propriedades específicas do óleo e do gás estão listadas na Tabela 2. O número total de partículas representando o óleo foi de 37.397; para o gás, foram utilizadas 12.162 partículas. O tempo máximo de simulação foi de 10 segundos.

Tabela 1 Parâmetros para as simulações

Propriedades	Unidade	Valor
C_I	-	0,066
C_S	-	0,12
g	m/s^2	9,81
L_c	m	0,14
N_s	-	40
Δl	m	0,002

Tabela 2 Propriedades do óleo e do gás

Propriedades	Unidade	Óleo	Gás
c_s	m/s	100	343,28
γ	-	7	1,32
μ	N.s/m^2	0,0092	0,000275
ρ_0	kg/m^3	728	0,717

Simulamos dois casos: um sem injeção de gás e outro com injeção contínua de gás até o tempo final estipulado. Os resultados são apresentados, respectivamente, nas Figuras 2–5 e 6–9. Tanto o óleo quanto o gás foram postos em movimento por meio do deslocamento de um pistão com velocidade especificada, recurso disponível na versão do DualSPHysics utilizada.

Devido ao alto custo computacional, as simulações foram realizadas utilizando a Application Programming Interface (API) CUDA da Nvidia para computação paralela em Graphics Processing Units (GPUs), com o uso de uma placa de vídeo Nvidia K80.

Na primeira simulação, apenas a fase óleo (partículas vermelhas) foi considerada, sem injeção de gás. Essa configuração serviu como referência para avaliarmos o impacto da injeção de gás. O deslocamento das partículas de óleo pode ser observado nas Figuras 2–5, para quatro instantes de tempo predefinidos, com a velocidade do pistão estabelecida em 0,01 m/s.

No segundo caso, o gás foi injetado continuamente com uma velocidade do pistão de 0,025m/s durante todo o período de escoamento do óleo, Figuras 6–9, para os mesmos instantes de tempo considerados anteriormente. Ressaltamos que o gás se expande dentro do tanque de separação.

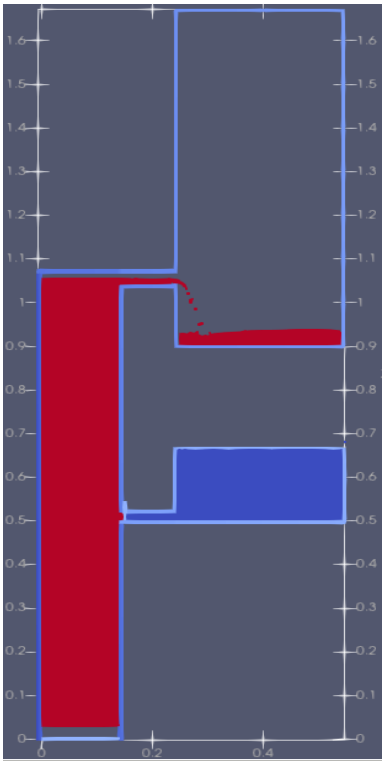

Figura 2: Escoamento da fase óleo sem a injeção de gás: t=2,5 s

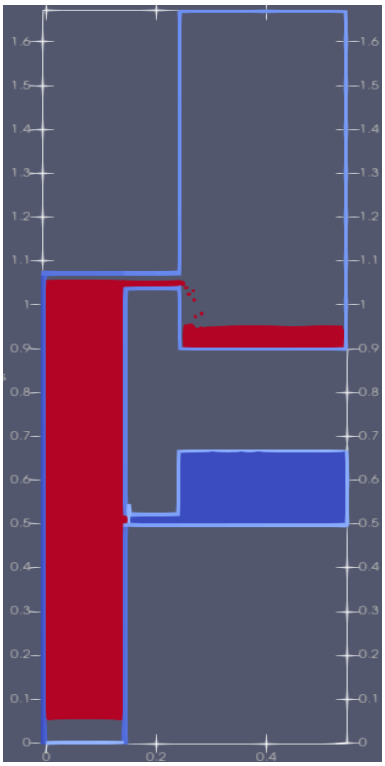

Figura 3: Escoamento da fase óleo sem a injeção de gás: t=5,0 s

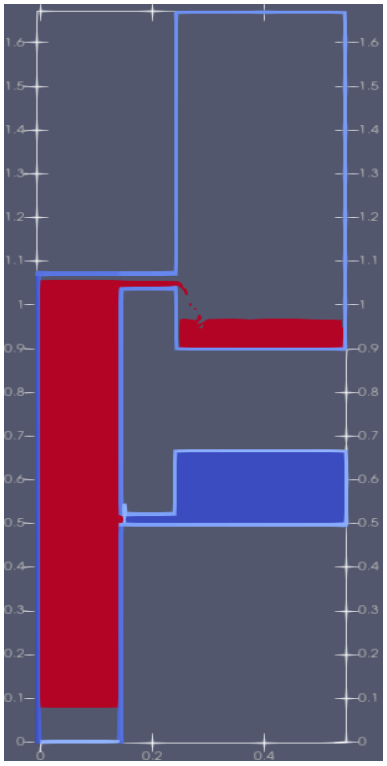

Figura 4: Escoamento da fase óleo sem a injeção de gás: t=7,5 s

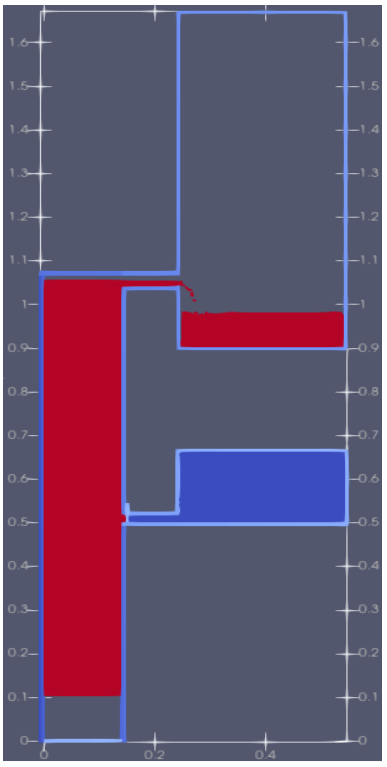

Figura 5: Escoamento da fase óleo sem a injeção de gás: t=10,0 s

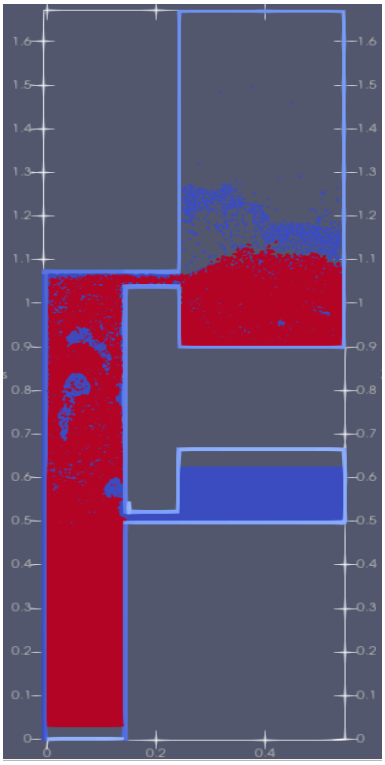

Figura 6: Escoamento da fase óleo com a injeção contínua de gás: t=2,5 s

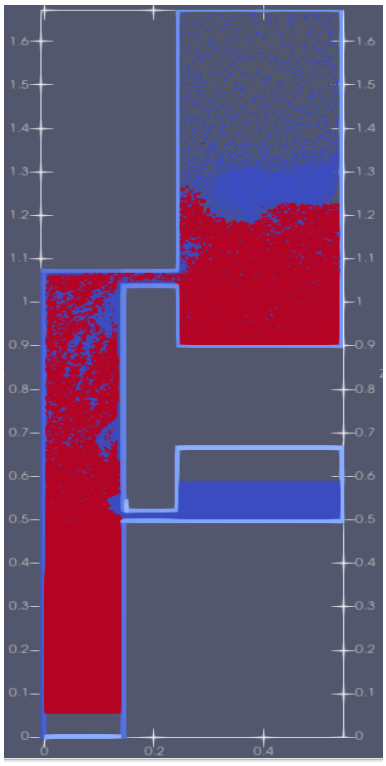

Figura 7: Escoamento da fase óleo com a injeção contínua de gás: t=5,0 s

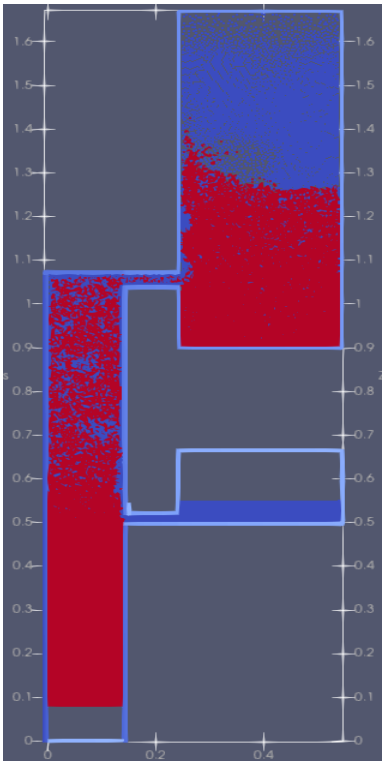

Figura 8: Escoamento da fase óleo com a injeção contínua de gás: t=7,5 s

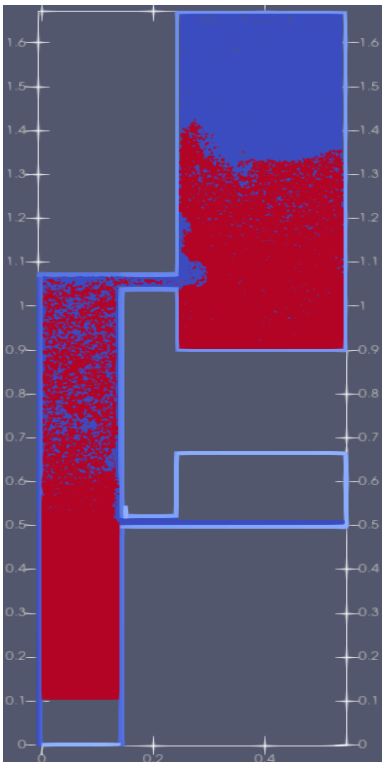

Figura 9: Escoamento da fase óleo com a injeção contínua de gás: t=10,0 s

Em função da distribuição das fases, foi possível observar que a produção de óleo aumentou significativamente com a aplicação da técnica de gas lift. Essa constatação foi feita por meio da estimativa do volume de óleo, ao final dos 10 segundos, contido no reservatório de separação. Como os valores de massa específica de cada partícula estão disponíveis em todos os instantes da simulação, o volume de fluido pôde ser calculado pela relação $V = m/\rho$, considerando que a massa das partículas é constante. Utilizamos essa relação para computar o volume de óleo no tanque de separação e verificamos que ele foi quatro vezes maior do que no caso sem a injeção contínua de metano.

6 Conclusões

Neste trabalho, empregamos o método Smoothed Particle Hydrodynamics na simulação numérica do escoamento multifásico em um duto, com foco na técnica de recuperação gas lift. O escoamento isotérmico bifásico óleo-gás foi estudado a fim de verificarmos se o método seria capaz de reproduzir o comportamento físico esperado durante a injeção de gás para aumentar o volume de óleo extraído.

Como resultado, o método SPH da versão multifásica da distribuição atual do DualSPHysics permitiu confirmar, ainda que qualitativamente, um maior volume de óleo coletado no tanque separador do sistema, ao compararmos os valores obtidos sem e com a injeção contínua de gás, para o mesmo intervalo de tempo. Esse resultado sugere que o método é adequado para a simulação de escoamentos multifásicos em dutos verticais e, em particular, na aplicação da técnica de elevação artificial.

Em conclusão, constatamos que a versão multifásica do DualSPHysics pode ser utilizada na simulação da técnica de elevação por injeção de gás. No entanto, modificações adicionais, como a implementação de condições de contorno do tipo inlet e outlet, devem ser exploradas para dispensar o uso de pistões e do tanque de separação.

Como perspectiva futura, também estamos trabalhando na resolução do mesmo problema utilizando o método Volume of Fluid, na versão disponibilizada no OpenFOAM.

Referências

[1] M. Abdulkadir, V. Hernandez-Perez, S. Lo, I.S. Lowndes, and B.J. Azzopardi. Comparison of experimental and computational fluid dynamics (CFD) studies of slug flow in a vertical riser. Experimental Thermal and Fluid Science, 68:468–483, 2015.

[2] G. K. Batchelor. An Introduction to Fluid Dynamics. Cambridge Mathematical Library. Cambridge University Press, 2000.

[3] G. Boyun, W. C. Lyons, and A. Ghalambor. Petroleum Production Engineering - A Computer-Assisted Approach. Elsevier Science & Technology Books, 2007.

[4] Naim Carvalho, Grazione de Souza, and Helio Pedro Amaral Souto. Simulação numérica do escoamento bifásico óleo-água em um duto horizontal empregando o método Smoothed Particle Hydrodynamics. VETOR - Revista de Ciências Exatas e Engenharias, 31(2):14–24, 2021.

[5] Clodoaldo de Oliveira Carvalho Filho. Produção de petróleo por elevação a gás intermitente: simulação e análise dos métodos convencional e invertido. PhD thesis, Universidade Estadual de Campinas, 2004.

[6] A.J.C. Crespo, J.M. Domínguez, B.D. Rogers, M. Gómez-Gesteira, S. Longshaw, R. Canelas, R. Vacondio, A. Barreiro, and O. García-Feal. Dualsphysics: Open-source parallel cfd solver based on smoothed particle hydrodynamics (sph). Computer Physics Communications, 187:204–216, 2015.

[7] S. Márquez Damián. An extended mixture model for the simultaneous treatment of short and long scale interfaces. PhD thesis, Instituto de Desarrollo Tecnologico para la Industria Quimica, 2013.

[8] Naim Jessé dos Santos Carvalho. Simulação numérica do escoamento bifásico em um duto horizontal empregando o método smoothed particle hydrodynamics. Master's thesis, Programa de Pós-Graduação em Modelagem Computacional, Universidade do Estado do Rio de Janeiro, Nova Friburgo, Brasil, 2021.

[9] Thomas Douillet-Grellier, Florian De Vuyst, Henri Calandra, and Philippe Ricoux. Simulations of intermittent two-phase flows in pipes using Smoothed Particle Hydrodynamics. Computers & Fluids, 177:101 – 122, 2018.

[10] Carlos Alberto Dutra Fraga Filho. Smoothed Particle Hydrodynamics: Fundamentals and Basic Applications in Continuum Mechanics. Springer, 2019.

[11] H. Gotoh, T. Shibahara, and T. Sakai. Subparticle-scale turbulence model for the mps method. Computational Fluid Dynamics Journal, 9:339–347, 2001.

[12] L. A. O. Guerra, B. O. Temer, J. B. R Loureiro, and A. P. Freire. Experimental study of gas-lift system with inclined gas jets. Journal of Petroleum Science and Engineering, 216(110749), 2022.

[13] A. Hernandez. Fundamentals of Gas Lift Engineering: Well Design and Troubleshooting. Elsevier Science, 2016.

[14] Mohamed M. Hussein, A. Al-Sarkhi, H. M. Badr, and M. A. Habib. CFD modeling of liquid film reversal of two-phase flow in vertical pipes. Journal of Petroleum Exploration and Production Technology, 9(4):3039–3070, 2019.

[15] Bruno Lafaurie, Ruben Scardovelli, Carlo Nardone, Stephane Zaleski, and Gianluigi Zanetti. Modelling merging and fragmentation in multiphase flows with SURFER. Journal of Computational Physics, 113(1):134–147, 1994.

[16] G. Liu and M. Liu. Smoothed Particle Hydrodynamics: A Meshfree Particle Method. World Scientific Publishing Company, 2003.

[17] Athanasios Mokos. Muti-phase Modelling of Violent Hydrodynamics using Smoothed Particle Hydrodynamics (SPH) on Graphics Processing Units (GPU). PhD thesis, School of Mechanical, Aerospace and Civil Engineering, Faculty of Engineering and Physical Sciences, University of Manchester, Manchester, 2013.

[18] J. J Monaghan. Simulating free surface flows with SPH. Journal of Computational Physics, 110(2):399–406, 1994.

[19] M. Parsi, R. E. Vieira, M. Agrawal, V. Srinivasan, B. S. McLaury, S. A. Shirazi, E. Schleicher, and U. Hampel. Computational fluid dynamics (CFD) simulation of multiphase flow and validating using wire mesh sensor. In International Conference on Multiphase Production Technology, pages BHR–2015–D4, Cannes, France, June 2015.

[20] Haroldo dos Santos Rizzo Filho. A otimização de gás lift na produção de petróleo: avaliação da curva de performance do poço. Master's thesis, Universidade Federal do Rio de Janeiro, 2011.

[21] Nagham Amer Sami and Zoltan Turzo. Computational fluid dynamic (CFD) modelling of transient flow in the intermittent gas lift. Petroleum Research, 5(2):144–153, 2020.

[22] Ovadia Shoham. Mechanistic Modeling of Gas-liquid Two-phase Flow in Pipes. Society of Petroleum Engineers, 2013.

[23] Yemada Taitel and A. E. Dukler. A model for predicting flow regime transitions in horizontal and near horizontal gas-liquid flow. AICHE Journal, 22(1):47–55, 1976.

[24] Alex Furtado Teixeira. Otimização da produção de poços de petróleo com gas lift contínuo. Master's thesis, Universidade Federal do Rio de Janeiro, 2013.

[25] F. Tocci, F. Bos, and R. Henkes. CFD for multiphase flow in vertical risers. In International Conference on Multiphase Production Technology, pages BHR–2017–309, Cannes, France, June 2017.

[26] Loup Verlet. Computer "experiments" on classical fluids - thermodynamical properties of lennard-jones molecules. Physical Review, 159(1):98–103, 1967.

[27] Kent E. Wardle and Henry G. Weller. Hybrid multiphase CFD solver for coupled dispersed/segregated flows in liquid-liquid extraction. International Journal of Chemical Engineering, 2013(2):13, 2013.

[28] H. Wendland. Piecewise polynomial, positive definite and compactly supported radial functions of minimal degree. Advances in Computational Mathematics, 4:389–396, 1995.

Numerical Simulation of Water-Gas Flow in Low Permeability Reservoirs

Gillyan Macário da Silva

Pós-graduação em Modelagem Computacional, Instituto Politécnico, Universidade do Estado do Rio de Janeiro, Brasil.

Mayksoel Medeiros de Freitas

Departamento de Engenharia Mecânica e Energia, Instituto Politécnico, Universidade do Estado do Rio de Janeiro, Brasil.

Grazione de Souza

Departamento de Modelagem Computacional, Instituto Politécnico, Universidade do Estado do Rio de Janeiro, Brasil.

Helio Pedro Amaral Souto

Departamento de Modelagem Computacional, Instituto Politécnico, Universidade do Estado do Rio de Janeiro, Brasil.

Abstract: Natural gas recovery has increased with the production from unconventional reservoirs with low absolute permeability. In these reservoirs, production is favored, for example, by the use of horizontal wells and the gas-phase slippage effect. This work performs a numerical simulation of two-phase isothermal water-gas flow, accounting for the impact of gas slip and permeability variation as a function of the stress change acting on the porous matrix. The governing equations are discretized using the Finite Volume Method. The obtained algebraic equation systems are linearized and solved by applying a Picard-Newton solution strategy, an operator splitting method, and the iterative preconditioned Stabilized Biconjugate Gradient method. The results are presented in terms of instantaneous gas flow rate and recovered gas volume, considering several production scenarios for the prescribed well pressure. In conclusion, the results showed that it was possible to capture the incorporated physical effects, with slippage favoring production and the change due to the stress effect leading to a decrease in apparent permeability resulting from the pressure drop caused by production.

Palavras-chave: horizontal well, low permeability reservoirs, Picard-Newton method, two-phase flow.

Corresponding author: Helio Pedro Amaral Souto, helio@iprj.uerj.br

Received: 08 Jul 2025 / Accepted: 20 Jul 2025 / Published: 11 Aug 2025.

1 Introduction

The increasing global energy demand has driven the exploration and production of unconventional oil and gas sources [4]. Among the significant available resources are gas reservoirs characterized by low permeability, often referred to as tight gas reservoirs. Production from these reservoirs presents unique challenges due to their inherent low permeability and porosity, as well as their structural complexity [1, 17]. To overcome these difficulties and make production viable, advanced techniques like hydraulic fracturing and horizontal drilling are widely employed [8]. Furthermore, multiphase flow introduces additional complications [21], such as production limitations caused by the presence of water, which can occupy pore spaces and impede gas flow [5].

According to Xu et al. [23], the presence of water in pores and fractures significantly interferes with gas mobility in a two-phase flow context. Typically, numerical methods are utilized to study flow dynamics and predict production. The most sophisticated models integrate elements such as gas adsorption on the rock surface and incorporate mechanisms that account for gas slippage. Moreover, the injection of fluids during fracturing can alter reservoir properties, potentially creating low-permeability zones near the wellbore [15].

Several mechanisms in physical-mathematical modeling can explain the low water recovery often observed during production in these reservoirs. These include wa-

ter retention within the fracture network and water imbibition associated with osmotic and capillary pressure. As highlighted by He et al. [15], these factors hinder water flow, a phenomenon that can be effectively modeled using a modified version of Darcy's law for low-velocity flows. Consequently, the authors adapted Darcy's law to describe water transport and employed another version adjusted for gas transport, specifically considering slippage mechanisms and free molecular flow. The Klinkenberg effect, also known as gas slippage, occurs in low-permeability media where gas molecules achieve higher velocities near pore walls. This phenomenon is particularly relevant under low-pressure conditions and results in an effective (apparent) permeability that is greater than the absolute permeability [18].

On the other hand, effective stress can significantly impact the permeability of porous media. Compression of the porous medium, caused by increased pressure, can restrict fluid flow. This necessitates incorporating a relationship that describes permeability as a function of stress and deformation [22]. These effects become especially important in horizontal wells with hydraulic fracturing, where stress redistribution can alter flow behavior within open fractures. In contrast, conventional reservoirs typically trap hydrocarbons in porous and permeable rocks, generally allowing for natural migration and facilitated extraction.

Indeed, horizontal drilling represents an essential technology in the exploitation of unconventional reservoirs. It has radically transformed the oil and gas industry by enabling production from geological formations with inherently low permeability [2]. This technique involves diverting the well trajectory from a vertical to a horizontal or near-horizontal orientation relative to the main reservoir bedding, thereby maximizing the contact area between the well and the producing formation. Initially, the well is drilled vertically until it reaches a depth close to the target layer. Subsequently, a directional deviation is performed using specialized tools to change the well's trajectory. From this point, drilling continues horizontally along the producing layer for hundreds or even thousands of meters, significantly expanding the hydrocarbon drainage area.

In this work, we study two-phase water-gas flow during production in a low-permeability reservoir utilizing a horizontal well and numerical reservoir simulation techniques. Our primary contribution lies in addressing this challenging problem by proposing a novel solution approach: we employ the Picard-Newton method to accurately model situations where both slippage and stress effects significantly influence the apparent permeability.

2 Physical-mathematical modeling

Considering the Cartesian coordinate system, the mass balance for flow in porous media yields [7],

$$\frac{\partial}{\partial t}\left(\phi\rho_l S_l\right) + \nabla\cdot\left(\rho_l \mathbf{v}_l\right) - \dot{q}_{ml} = 0, \tag{1}$$

where ϕ is the porosity, and ρ_l, S_l, $\mathbf{v}_l$, and $\dot{q}_{ml}$ are, respectively, the specific mass, saturation, apparent velocity, and source term (mass per unit time per unit volume) for phase l.

For multiphase flows, the classical Darcy's law requires modification to account for the flow resistance that a given phase exerts on the others [11]. Furthermore, Darcy's law can be modified to incorporate effects such as slippage and the influence of effective stress.

Slippage, also known as the Klinkenberg effect, occurs when the pore size is comparable to the mean free path of gas molecules, with the effect being more noticeable at reduced pressures. The permeability value in these cases must be corrected, with the first model employed to capture this phenomenon being [18]

$$\mathbf{k}_{ag} = \left(1 + \frac{b}{p}\right)\mathbf{k}, \tag{2}$$

where $\mathbf{k}_{ag}$ is the apparent gas permeability, $\mathbf{k}$ the intrinsic permeability of the porous medium, p the gas pressure, and b the Klinkenberg factor.

On the other hand, in certain situations, permeability can be sensitive to variations in stress, which influences fluid flow within these formations. This phenomenon is known as the effective stress effect on permeability and can significantly impact gas production [14]. A simplified model used in the modeling of this effect is given by [25]

$$\mathbf{k} = e^{-\gamma(p_0 - p)}\mathbf{k}_0, \tag{3}$$

where γ is the permeability modulus, dependent on the mineral composition and mechanical characteristics of the rock [24], p_0 is the initial pressure, and $\mathbf{k}_0$ represents the initial permeability (tensor considered diagonal here).

The concept of apparent permeability will be adopted for both phases. For the gas phase, $\mathbf{k}_{ag}$ takes into account the effects of slippage and effective stress, while for the water phase, $\mathbf{k}_{aw}$ considers only the effective stress effect. Thus, the modified Darcy's law is considered here in the form

$$\mathbf{v}_l = -\frac{k_{rl}}{\mu_l}\mathbf{k}_{al}\left(\nabla p_l - \lambda_l \nabla z\right) \tag{4}$$

where $\mathbf{k}_{al}$ is the apparent permeability tensor, p_l, μ_l, and k_{rl} are, respectively, the pressure, viscosity, and relative permeability of phase l, $\lambda_l = \rho_l g$, and ∇z is the depth gradient, with g being the magnitude of gravitational acceleration.

Substituting Equation (4) into Equation (1),

$$\nabla\cdot\left[\frac{\rho_l k_{rl}}{\mu_l}\mathbf{k}_{al}\left(\nabla p_l - \lambda_l\nabla z\right)\right] = \frac{\partial}{\partial t}\left(\phi\rho_l S_l\right) - \dot{q}_{ml} \tag{5}$$

for each phase l, where w represents the wetting phase (water), and n designates the non-wetting phase (gas).

Expressing the specific mass of the phase in terms of the Formation Volume Factor (FVF), Equation (5) can be rewritten as [13]

$$\nabla\cdot\left[\frac{k_{rl}}{\mu_l B_l}\mathbf{k}_{al}\left(\nabla p_l - \lambda_l\nabla z\right)\right] = \frac{\partial}{\partial t}\left(\frac{\phi S_l}{B_l}\right) - \dot{q}_{scl} \tag{6}$$

where B_l is the FVF of phase l and $\dot{q}_{scl} = \dot{q}_{ml}/\rho_{scl}$, with $\dot{q}_{scl}$ being a volumetric flow rate source term under standard conditions and ρ_{scl} the specific mass under standard conditions of phase l.

Assuming that the medium is fully saturated, we have [11],

$$S_{\mathtt{w}} + S_{\mathtt{g}} = 1, \tag{7}$$

where $S_{\mathtt{w}}$ is the saturation of the wetting phase and $S_{\mathtt{g}}$ is the saturation of the non-wetting phase.

Now, from the equation that provides the capillary pressure as a function of the phase pressures [7],

$$p_c = p_{\mathtt{g}} - p_{\mathtt{w}}, \tag{8}$$

the water pressure can be written in terms of the gas pressure and the capillary pressure.

From Equation (6), $S_{\mathtt{g}} = 1 - S_{\mathtt{w}}$, and $p_{\mathtt{w}} = p_{\mathtt{g}} - p_c$, we obtain for the gas phase

$$\nabla \cdot \left[\frac{k_{r\mathtt{g}}}{\mu_{\mathtt{g}} B_{\mathtt{g}}} \mathbf{k}_{ag} \left(\nabla p_{\mathtt{g}} - \lambda_{\mathtt{g}} \nabla z \right) \right] = \frac{\partial}{\partial t} \left[\frac{\phi(1 - S_{\mathtt{w}})}{B_{\mathtt{g}}} \right] - \dot{q}_{sc\mathtt{g}} \tag{9}$$

and, for the water phase,

$$\nabla \cdot \left[\frac{k_{r\mathtt{w}}}{\mu_{\mathtt{w}} B_{\mathtt{w}}} \mathbf{k}_{aw} \left(\nabla p_{\mathtt{g}} - \nabla p_c - \lambda_{\mathtt{w}} \nabla z \right) \right] = \frac{\partial}{\partial t} \left(\frac{\phi S_{\mathtt{w}}}{B_{\mathtt{w}}} \right) - \dot{q}_{sc\mathtt{w}}, \tag{10}$$

where it was considered that $w = \mathtt{w}$ (water) and $n = \mathtt{g}$ (gas).

In this work, the modified Corey model is employed for the wetting phase [11], such that

$$k_{r\mathtt{w}}(S_{\mathtt{w}}) = k_{r\mathtt{w}_{max}} \left(\frac{S_{\mathtt{w}} - S_{i\mathtt{w}}}{1 - S_{i\mathtt{w}} - S_{gr\mathtt{w}}} \right)^{e\mathtt{w}} \tag{11}$$

and, for the non-wetting phase,

$$k_{r\mathtt{g}}(S_{\mathtt{w}}) = k_{r\mathtt{g}_{max}} \left(\frac{1 - S_{\mathtt{w}} - S_{gr\mathtt{w}}}{1 - S_{i\mathtt{w}} - S_{gr\mathtt{w}}} \right)^{eo\mathtt{w}}, \tag{12}$$

where $S_{\mathtt{w}}$ and $S_{i\mathtt{w}}$ represent, in this order, the saturation and irreducible saturation of the wetting phase, $S_{gr\mathtt{w}}$ is the residual saturation of the non-wetting phase, $kr\mathtt{w}_{max}$ is the maximum water saturation, $kr\mathtt{g}_{max}$ is the maximum gas saturation, $e\mathtt{w}$ and $eo\mathtt{w}$ are the Corey exponents for the water and gas phases, respectively.

The adopted capillary pressure curve originates from models based on power laws [12],

$$p_c(S_{\mathtt{w}}) = p_{c_{max}} \left(\frac{1 - S_{\mathtt{w}} - S_{gr\mathtt{w}}}{1 - S_{i\mathtt{w}} - S_{gr\mathtt{w}}} \right)^{epc}, \tag{13}$$

where the maximum value of the curve, $p_{c_{max}}(S_{i\mathtt{w}})$, and the exponent epc must be determined from experiments or through field data.

The initial condition is defined for an arbitrary time t_0. For example, for the variables $p_g = p(x, y, z, t)$ and $S_w = S(x, y, z, t)$, the initial condition is imposed in the form [7]:

$$p(x, y, z, t_0) = p_0(x, y, z) \qquad \text{in the entire } \Omega \tag{14}$$

and

$$S(x, y, z, t_0) = S_0(x, y, z) \qquad \text{in the entire } \Omega, \tag{15}$$

in which S_0 represents the saturation throughout the domain Ω at the initial time.

In petroleum reservoir simulations, it is common to define initial pressures at a given reference depth. Then, the hydrostatic gradient and capillary effects are used to determine the initial values at different reservoir depths [11, 13]. Regarding the boundary conditions, in this work, no-flow conditions are imposed at the reservoir boundaries. Finally, more details on the calculations associated with fluid and rock properties can be found in [13].

3 Numerical Solution Methodology

We now proceed to the presentation of the numerical solution methodology employed in this work, which includes the use of the Finite Volume Method, operator splitting, linearizations, a well-reservoir coupling technique, and an iterative method for solving linear systems.

3.1 Discretization

In the Finite Volume Method, the non-linear partial differential equations (PDEs) that govern the flow are first integrated in space and time over a finite volume. This procedure ensures that mass and fluxes are conserved in each finite volume and over the entire domain [6]. In this method, the solution domain is divided into finite volumes (cells or blocks) with known, not necessarily equal, dimensions. Within this framework, the average values of pressure and saturation are determined at the centers of the blocks. In the three-dimensional case, each finite volume is represented by a parallelepiped with lengths Δx, Δy, and Δz, in that order, such that

$$\sum_{i=1}^{n_x} \Delta x_i = L_x, \quad \sum_{j=1}^{n_y} \Delta y_j = L_y, \quad \sum_{k=1}^{n_z} \Delta z_k = L_z, \tag{16}$$

where L_x, L_y, and L_z represent the spatial dimensions of the reservoir, as illustrated in Figure 1. The reservoir is partitioned using a grid composed of n_x, n_y, and n_z volumes in the directions of the x, y, and z axes, respectively. The indices i, j, and k represent the centers of the blocks in the x, y, and z directions, and their faces are identified by $i \pm 1/2, j, k$, $i, j \pm 1/2, k$, and $i, j, k \pm 1/2$. The commonly used compact notation [13] was adopted, in which the faces of the finite volumes are identified by lowercase letters: $(i - 1/2, j, k) = w$, $(i + 1/2, j, k) = e$,

$(i, j-1/2, k) = n$, $(i, j+1/2, k) = s$, $(i, j, k-1/2) = a$, and $(i, j, k+1/2) = b$ (Figure 2). In the computational grid, the center of block P has coordinates (i, j, k), and for neighboring volumes, we have $(i-1, j, k) = W$, $(i+1, j, k) = E$, $(i, j+1, k) = N$, $(i, j-1, k) = S$, $(i, j, k-1) = B$, and $(i, j, k+1) = A$.

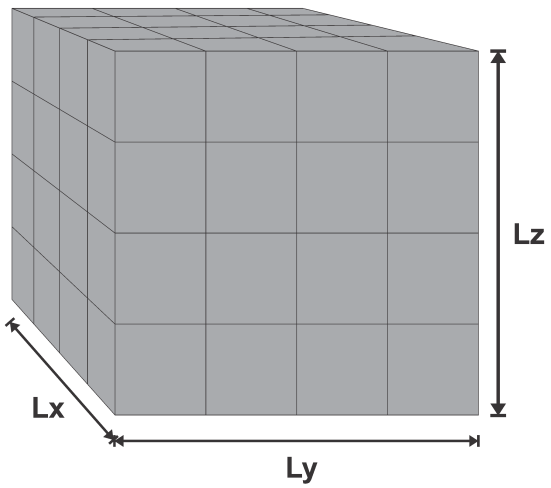

Figure 1: Three-dimensional grid.

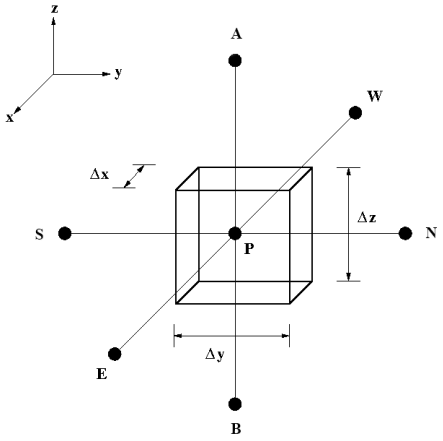

Figure 2: Finite Volume.

The discretization of Equations (9) and (10) begins with an integration over a control volume, as illustrated in Figure 2. Considering the standard development and employing three-point centered difference approximations, their spatially discretized forms are obtained [13]

$$\frac{\partial}{\partial t}\left[\frac{\phi(1-S_{\mathtt{w}})}{B_{\mathtt{g}}}\right]_P V_P = \Delta\left(T_{\mathtt{g}}\Delta p_{\mathtt{g}}\right)_P - \Delta\left(T_{\mathtt{g}}\lambda_{\mathtt{g}}\Delta z\right)_P + q_{scg_P} \tag{17}$$

and

$$\frac{\partial}{\partial t}\left(\frac{\phi S_{\mathtt{w}}}{B_{\mathtt{w}}}\right)_P V_P = \Delta\left(T_{\mathtt{w}}\Delta p_{\mathtt{g}}\right)_P - \Delta\left(T_{\mathtt{w}}\Delta p_c\right)_P - \Delta\left(T_{\mathtt{w}}\lambda_{\mathtt{w}}\Delta z\right)_P + q_{scw_P}, \tag{18}$$

where $V_P = \Delta x_P \Delta y_P \Delta z_P$, $q_{scl_P} = \dot{q}_{scl_P} V_P$, and the operator $\Delta\left(\xi\Delta\eta\right)_P$ was used [11]

$$\Delta\left(\xi\Delta\eta\right)_P \equiv \xi_{x_w}\left(\eta_W - \eta_P\right) + \xi_{x_e}\left(\eta_E - \eta_P\right) + \xi_{y_n}\left(\eta_N - \eta_P\right) + \xi_{y_s}\left(\eta_S - \eta_P\right) + \xi_{z_a}\left(\eta_A - \eta_P\right) + \xi_{z_b}\left(\eta_B - \eta_P\right), \tag{19}$$

and, for two-phase flow, the transmissibilities T_{lx_f} [11] were introduced into Equations (17) and (18):

$$T_{lx_f} \equiv \left(\frac{k_{alx}A_x k_{rl}}{\mu_l B_l \Delta x}\right)_f \qquad l = \mathtt{g}, \mathtt{w}, \tag{20}$$

for $f = w$ or $f = e$. Analogous expressions for transmissibilities can be defined for the y and z directions.

Next, the accumulation terms of Equations (9) and (10) are considered,

$$\frac{\partial}{\partial t}\left[\frac{\phi(1-S_{\mathtt{w}})}{B_g}\right] = \left[\phi\frac{d}{dp_{\mathtt{g}}}\left(\frac{1}{B_{\mathtt{g}}}\right)\right](1-S_{\mathtt{w}})\frac{\partial p_{\mathtt{g}}}{\partial t} + \left[\frac{1}{B_{\mathtt{g}}}\frac{d\phi}{dp_{\mathtt{g}}}\right](1-S_{\mathtt{w}})\frac{\partial p_{\mathtt{g}}}{\partial t} - \left(\frac{\phi}{B_{\mathtt{g}}}\right)\frac{\partial S_{\mathtt{w}}}{\partial t} \tag{21}$$

and

$$\frac{\partial}{\partial t}\left(\frac{\phi S_{\mathtt{w}}}{B_{\mathtt{w}}}\right) = \left[\phi\frac{d}{dp_{\mathtt{w}}}\left(\frac{1}{B_{\mathtt{w}}}\right) + \frac{1}{B_{\mathtt{w}}}\frac{d\phi}{dp_{\mathtt{w}}}\right]S_{\mathtt{w}}\frac{\partial p_{\mathtt{w}}}{\partial t} + \left(\frac{\phi}{B_{\mathtt{w}}}\right)\frac{\partial S_{\mathtt{w}}}{\partial t}. \tag{22}$$

Disregarding the variation of capillary pressure with time [13], $\partial p_c/\partial t = 0$, we have $\partial p_{\mathtt{w}}/\partial t \approx \partial p_{\mathtt{g}}/\partial t$; therefore,

$$\frac{\partial}{\partial t}\left[\frac{\phi(1-S_{\mathtt{w}})}{B_{\mathtt{g}}}\right] = \left[\phi\left(\frac{1}{B_{\mathtt{g}}}\right)' + \frac{\phi'}{B_{\mathtt{g}}}\right](1-S_{\mathtt{w}})\frac{\partial p_{\mathtt{g}}}{\partial t} - \left(\frac{\phi}{B_{\mathtt{g}}}\right)\frac{\partial S_{\mathtt{w}}}{\partial t} \tag{23}$$

and

$$\frac{\partial}{\partial t}\left(\frac{\phi S_{\mathtt{w}}}{B_{\mathtt{w}}}\right) = \left[\phi\left(\frac{1}{B_{\mathtt{w}}}\right)' + \frac{\phi'}{B_{\mathtt{w}}}\right]S_{\mathtt{w}}\frac{\partial p_{\mathtt{g}}}{\partial t} + \left(\frac{\phi}{B_{\mathtt{w}}}\right)\frac{\partial S_{\mathtt{w}}}{\partial t}, \tag{24}$$

where $\phi' = \frac{d\phi}{dp_l}$ and $\left(\frac{1}{B_l}\right)' = \frac{d}{dp_l}\left(\frac{1}{B_l}\right)$, $l = \mathtt{g}, \mathtt{w}$ [11].

Substituting Equations (23) and (24) into the right-hand side of Equations (17) and (18) and integrating them in time, we obtain

$$\Delta\left(T_{\mathtt{g}}\Delta p_{\mathtt{g}}\right)_P^{n+1} - \Delta\left(T_{\mathtt{g}}\lambda_{\mathtt{g}}\Delta z\right)_P^{n+1}$$

$$= C_{\mathtt{g}p}\Delta_t p_{\mathtt{g}} + C_{\mathtt{g}s}\Delta_t S_{\mathtt{w}} - q_{sc\mathtt{g}_P}^{n+1} \tag{25}$$

and

$$\Delta\left(T_{\mathtt{w}}\Delta p_{\mathtt{g}}\right)_P^{n+1} - \Delta\left(T_{\mathtt{w}}\Delta p_c\right)_P^{n+1} - \Delta\left(T_{\mathtt{w}}\lambda_{\mathtt{w}}\Delta z\right)_P^{n+1}$$

$$= C_{\mathtt{w}p}\Delta_t p_{\mathtt{g}} + C_{\mathtt{w}s}\Delta_t S_{\mathtt{w}} - q_{sc\mathtt{w}_P}^{n+1} \tag{26}$$

where the coefficients C are given by

$$C_{\mathtt{g}p} = \frac{V_P}{\Delta t}\left\{\left[\phi_P^{n+1}\left(\frac{1}{B_{\mathtt{g}}}\right)_P' + \frac{\phi_P'}{B_{\mathtt{g}P}^n}\right](1 - S_{\mathtt{w}P}^n)\right\}, \tag{27}$$

$$C_{\mathtt{g}s} = -\frac{V_P}{\Delta t}\left(\frac{\phi_P^{n+1}}{B_{\mathtt{g}P}^{n+1}}\right), \tag{28}$$

$$C_{\mathtt{w}p} = \frac{V_P}{\Delta t}\left\{\left[\phi_P^{n+1}\left(\frac{1}{B_{\mathtt{w}}}\right)_P' + \frac{\phi_P'}{B_{\mathtt{w}P}^n}\right] S_{\mathtt{w}P}^n\right\}, \tag{29}$$

and

$$C_{\mathtt{w}s} = \frac{V_P}{\Delta t}\left(\frac{\phi_P^{n+1}}{B_{\mathtt{w}P}^{n+1}}\right), \tag{30}$$

and the operator $\Delta_t\varphi = \varphi_P^{n+1} - \varphi_P^n$ was used.

In Equations (27), (28), (29), and (30), the superscripts $n+1$ and n indicate the future and current time instants, respectively. Additionally, $\Delta t = t^{n+1} - t^n$, with ϕ, $S_{\mathtt{w}}$, and B_l evaluated at times n or $n+1$ to obtain a conservative approximation in the temporal integration [11]. Equations (25) and (26) therefore result in a fully implicit formulation.

It is assumed that the rocks have a small and constant compressibility. Thus, we have [11]

$$\phi = \phi^0\left[1 + c_\phi(p_{\mathtt{g}} - p^0)\right], \tag{31}$$

where c_ϕ is the rock compressibility and ϕ^0 is the porosity evaluated at the reference pressure p^0. The water phase is considered slightly compressible, such that

$$B_{\mathtt{w}} = \frac{B_{\mathtt{w}}^0}{1 + c_w(p_{\mathtt{w}} - p^0)}, \tag{32}$$

where $c_{\mathtt{w}}$ is the water compressibility and $B_{\mathtt{w}}^0$ is the FVF of water at the reference pressure p^0. From the definition of the FVF and the real gas law, $B_{\mathtt{g}}$ can be written as [12]

$$B_{\mathtt{g}} = \frac{p_{sc}}{T_{sc}}Z\frac{T}{p_{\mathtt{g}}}, \tag{33}$$

where p_{sc} and T_{sc} are, respectively, the pressure and temperature at standard conditions, and Z is the compressibility factor.

From Equation (31), it is possible to write

$$\phi' = c_\phi\phi^0. \tag{34}$$

Thus, considering Equations (32) and (33),

$$\left(\frac{1}{B_{\mathtt{w}}}\right)' = \frac{c_{\mathtt{w}}}{B_{\mathtt{w}}}, \tag{35}$$

$$\left(\frac{1}{B_{\mathtt{g}}}\right)' = \frac{1}{B_{\mathtt{g}}}\left(\frac{1}{p_{\mathtt{g}}} - \frac{1}{Z}\frac{dZ}{dp_{\mathtt{g}}}\right). \tag{36}$$

Equations (25) and (26) evaluated at the grid volumes form a coupled and non-linear system of algebraic equations. The implementation of the initial and boundary conditions follows the procedures adopted in [13].

Let it_{n-1} be the number of iterations required for the convergence of the solution at the previous time step Δt_{n-1}. As proposed by [19] and adapted by [13], an empirical criterion is used for the calculation of Δt, given by

$$\Delta t_n = \begin{cases} n_{decr}\Delta t_{n-1} \text{ if } & it_{n-1} > it_{decr}, \\ n_{incr}\Delta t_{n-1} \text{ if } & it_{n-1} \leq it_{incr}, \\ \Delta t_{n-1} & \text{otherwise}, \end{cases} \tag{37}$$

where n_{decr} and n_{incr} are the decrease and increase rates of the time step, with the iteration number limits established by it_{decr} and it_{incr} ($it_{incr} < it_{decr}$). An upper limit is also imposed on the time step, $\Delta t_n \leq \Delta t_{max}$. If the simulation does not converge, the step is reduced, allowing the continuation of the numerical simulation execution.

3.2 Well-Reservoir Coupling

In the adopted well-reservoir coupling model, a horizontal well with radius r_{wf} is considered, and frictional losses and inertial effects within the well are neglected [11]. For each finite volume c traversed by the well, with $c \in \psi_{wf}$, the flow rates of the non-wetting and wetting phases are expressed by [3]:

$$q_{sc\mathtt{g}_c} = -J_{\mathtt{g}_c}\left(p_{\mathtt{g}_c} - p_{wf_c}\right) \tag{38}$$

and

$$q_{sc\mathtt{w}_c} = -J_{\mathtt{w}_c}\left(p_{\mathtt{g}_c} - p_{c_c} - p_{wf_c}\right), \tag{39}$$

where J_l ($l = \mathtt{g}, \mathtt{w}$) represents the productivity index [3] and

$$J_{l_c} = G_{wf_c}\left(\frac{k_{rl_c}}{\mu_{l_c}B_{l_c}}\right). \tag{40}$$

For horizontal wells (parallel to the x direction) [3]

$$G_{wf_c} = \frac{2\pi\sqrt{k_{alz_c}k_{aly_c}}\Delta x_c}{\left[1-\left(\frac{r_{wf}}{r_{eq_c}}\right)^2\right]\ln\left(\frac{r_{eq_c}}{r_{wf}}\right)} \tag{41}$$

where r_{eq} is the equivalent radius given by

$$r_{eq_c} = \sqrt{\frac{\Delta z_c \Delta y_c}{\pi}}\ \exp\left(-0,5\right). \tag{42}$$

Equations (38) and (39) apply to each block c that contains a section of the well ($c \in \psi_{wf}$), and the total flow rate for each phase is the sum of the flow rates of all layers [11],

$$q_{sc\mathtt{g}_{sp}} = -\sum_{c\in\psi_{wf}} J_{\mathtt{g}_c}\left(p_{\mathtt{g}_c} - p_{wf_c}\right) \tag{43}$$

and

$$q_{sc\mathtt{w}_{sp}} = -\sum_{c\in\psi_{wf}} J_{\mathtt{w}_c}\left(p_{\mathtt{g}_c} - p_{c_c} - p_{wf_c}\right). \tag{44}$$

The total production flow rate is obtained by summing the flow rates of all layers, considering both phases [11],

$$q_{sc_{sp}} = -\sum_{c\in\psi_{wf}} J_{\mathtt{g}_c}\left(p_{\mathtt{g}_c} - p_{wf_c}\right) - \sum_{c\in\psi_{wf}} J_{\mathtt{w}_c}\left(p_{\mathtt{g}_c} - p_{c_c} - p_{wf_c}\right), \tag{45}$$

with a production condition in terms of prescribed pressure along the producing well, p_{wf}, being adopted in this work.

3.3 Linearizations

In this work, linearization techniques are employed, and the transmissibilities at the interfaces e, s, and b are defined, for example, for the x direction, as

$$T^{n+1}_{lx_e} = \left(\frac{k_{alx}A_x}{\Delta x}\right)_e \left(\frac{1}{\mu_l B_l}\right)^{n+1}_e k^{n+1}_{rl_e}, \tag{46}$$

for $l = \mathtt{g}, \mathtt{w}$, with analogous forms for the y and z directions. Similarly, their expressions at the w, n, and a faces can be written. They can also be represented as

$$T^{n+1}_{l_f} = G_f F^{n+1}_{p_f} F^{n+1}_{S_f} \tag{47}$$

where the term G_f depends on fluid, rock, and geometric properties, $F^{n+1}_{p_f}$ depends on pressure, and $F^{n+1}_{S_f}$ depends on saturation.

The terms $F^{n+1}_{p_f}$ and $F^{n+1}_{S_f}$ are taken to exemplify how the Picard and Newton-Raphson linearization methods are implemented.

We begin with the Picard iteration, where these terms are evaluated at time $n+1$, but at the previous iterative level v. As an example, we have

$$F^{n+1}_{p_e} \approx F^{n+1,v}_{p_e} \tag{48}$$

and

$$F^{n+1}_{S_e} \approx F^{n+1,v}_{S_e}, \tag{49}$$

and the method is conditionally stable [11], with a similar procedure used for the other interfaces.

When the Newton-Raphson method is used, the term at iteration $v+1$ is approximated from its value evaluated at the preceding iteration v [13], yielding, for example,

$$F^{n+1}_{p_e} \approx F^{n+1,v+1}_{p_e} \approx F^{n+1,v}_{p_e} + \left.\frac{\partial F_{p_e}}{\partial p_P}\right|^{n+1,v} \delta p^{n+1,v+1}_{n_P} + \left.\frac{\partial F_{p_e}}{\partial p_E}\right|^{n+1,v} \delta p^{n+1,v+1}_{n_E} \tag{50}$$

and

$$F^{n+1}_{S_e} \approx F^{n+1,v+1}_{S_e} \approx F^{n+1,v}_{S_e} + \left.\frac{\partial F_{p_e}}{\partial S_P}\right|^{n+1,v} \delta S^{n+1,v+1}_{w_P} + \left.\frac{\partial F_{p_e}}{\partial S_E}\right|^{n+1,v} \delta S^{n+1,v+1}_{w_E}, \tag{51}$$

with the properties at the e face determined based on the known values at nodes P and E. For the term $F^{n+1}_{S_e}$, the first-order upwind method is used. This method is unconditionally stable [11]. Regarding the accumulation terms, the non-linearities are considered weak (with the exception of gas flow) and are treated using the Picard method. On the other hand, the source terms require a linearization of the type employed for the transmissibilities.

3.4 Approximation at Finite Volume Faces

Since transmissibilities must be evaluated at the faces of the finite volumes and pressures and saturations are calculated at the center of the finite volumes, an interpolation must be employed in the calculation of the coefficients at the interfaces. Usually, arithmetic averages (in the case of volumes with the same dimension for the direction under analysis) are used for the pressure terms F_{p_f}, ensuring a second-order approximation [11]. For example, we have

$$F_{p_e} = \left(\frac{1}{\mu_l B_l}\right)_e = \frac{1}{2}\left[\left(\frac{1}{\mu_l B_l}\right)_E + \left(\frac{1}{\mu_l B_l}\right)_P\right]. \tag{52}$$

The first-order upwind method is used to prevent possible instabilities associated with centered differences [11] with respect to the saturation-dependent terms, F_{S_f}. For example, we use

$$k_{rl_e} = \begin{cases} k_{rl_P} \text{ if } \quad v_e \geq 0, \\ \\ k_{rl_E} \text{ if } \quad v_e < 0, \end{cases} \tag{53}$$

where v_e represents the velocity at the e face.

For the calculation of the term G_f, a harmonic average is used for the computation of the apparent permeability, based on what is generally applied for absolute permeability [11]. Considering the area perpendicular to the flow as constant, the geometric term at the e face can be expressed as

$$G_{x_e} = \left(\frac{k_{alx}A_x}{\Delta x}\right)_e = \frac{k_{alx_e}A_{x_e}}{\Delta x_e}, \tag{54}$$

where

$$k_{alx_e} = \frac{k_{alx_P}k_{alx_E}(\Delta x_P + \Delta x_E)}{k_{alx_P}\Delta x_E + k_{alx_E}\Delta x_P}. \tag{55}$$

Analogously, interpolations are performed at the w faces for the x direction, and at the n, s, a, and b faces, taking into account the y and z axes directions.

3.5 Hybrid Method

In the present work, the Hybrid Method described in [13] is used. Its objective is to improve numerical stability by implicitly solving, in separate steps, the algebraic systems associated with pressure and saturation. A fully implicit linearization for the wetting phase is employed via the Newton method, using an operator splitting technique [9, 16].

Similar to the Implicit Pressure Explicit Saturation (IMPES) method [11], the pressure equation for each volume can be obtained by combining Equations (25) and (26) such that the term $\Delta_t S_w$ is eliminated. This can be done by multiplying Equation (25) by $B_{\mathtt{g}_P}^{n+1}$, Equation (26) by $B_{\mathtt{w}_P}^{n+1}$, and adding them, noting that $B_{\mathtt{g}_P}^{n+1}C_{\mathtt{gs}} + B_{\mathtt{w}_P}^{n+1}C_{\mathtt{ws}} = 0$. Thus, the pressure equation can be written as [11]

$$\begin{aligned} &B_{\mathtt{g}_P}^{n+1}\Delta\left(T_{\mathtt{g}}\Delta p_{\mathtt{g}}\right)_P^{n+1} + B_{\mathtt{w}_P}^{n+1}\Delta\left(T_{\mathtt{w}}\Delta p_{\mathtt{g}}\right)_P^{n+1} \\ &-B_{\mathtt{w}_P}^{n+1}\Delta\left(T_{\mathtt{w}}\Delta p_c\right)_P^{n+1} - B_{\mathtt{g}_P}^{n+1}\Delta\left(T_{\mathtt{g}}\lambda_{\mathtt{g}}\Delta Z\right)_P^{n+1} \\ &+B_{\mathtt{w}_P}^{n+1}\Delta\left(T_{\mathtt{w}}\lambda_{\mathtt{w}}\Delta Z\right)_P^{n+1} \\ &=(B_{\mathtt{g}_P}^{n+1}C_{\mathtt{g}p} + B_{\mathtt{w}_P}^{n+1}C_{\mathtt{w}p})\Delta_t p_{\mathtt{g}} \\ &-(B_{\mathtt{g}_P}^{n+1}q_{sc\mathtt{g}_P}^{n+1} + B_{\mathtt{w}_P}^{n+1}q_{sc\mathtt{w}_P}^{n+1}), \end{aligned} \tag{56}$$

when calculating the pressures in the porous medium. Once determined at the current time step $(n+1)$ and iteration $(v+1)$, they cease to be unknowns when solving the wetting phase equation, making saturation the only variable to be computed. The fully implicit linearization, in terms of the wetting phase saturation, results in a system of equations that is solved by the Newton-Raphson method. This system can be represented in the following matrix form [13]:

$$\mathbf{J}_{\mathtt{w}}^{n+1,v}\boldsymbol{\delta}\mathbf{S}_{\mathtt{w}}^{n+1,v+1} = -\mathbf{R}_{\mathtt{w}}^{n+1,v}, \tag{57}$$

where $\mathbf{J}_{\mathtt{w}}^{n+1,v}$ represents the Jacobian matrix, $\boldsymbol{\delta}\mathbf{S}_{\mathtt{w}}^{n+1,v+1} = \mathbf{S}_{\mathtt{w}}^{n+1,v+1} - \mathbf{S}_{\mathtt{w}}^{n+1,v}$, and the vector containing the unknowns is

$$\mathbf{S}_{\mathtt{w}} = (S_{\mathtt{w}_1}, S_{\mathtt{w}_2}, S_{\mathtt{w}_3}, ..., S_{\mathtt{w}_N})^T, \tag{58}$$

while for the residual vector $\mathbf{R}_{\mathtt{w}}$ we have

$$\mathbf{R}_{\mathtt{w}} = (R_{\mathtt{w}_1}, R_{\mathtt{w}_2}, R_{\mathtt{w}_3}, ..., R_{\mathtt{w}_N})^T, \tag{59}$$

where $n = 1, 2, 3, ...N$, for a computational grid with N volumes.

After solving the system of linear algebraic equations, the new saturations can be calculated using

$$\mathbf{S}_{\mathtt{w}}^{n+1,v+1} = \mathbf{S}_{\mathtt{w}}^{n+1,v} + \boldsymbol{\delta}\mathbf{S}_{\mathtt{w}}^{n+1,v+1}, \tag{60}$$

applicable to each cell of the computational domain.

For each volume in the grid, using the Newton method, we have [13]

$$\begin{aligned} -R_{\mathtt{w}_P}^{n+1,v} = &\left.\frac{\partial R_{\mathtt{w}_P}}{\partial S_{\mathtt{w}_A}}\right|^{n+1,v} \delta S_{\mathtt{w}_A}^{n+1,v+1} \\ &+ \left.\frac{\partial R_{\mathtt{w}_P}}{\partial S_{\mathtt{w}_N}}\right|^{n+1,v} \delta S_{\mathtt{w}_N}^{n+1,v+1} \\ &+ \left.\frac{\partial R_{\mathtt{w}_P}}{\partial S_{\mathtt{w}_W}}\right|^{n+1,v} \delta S_{\mathtt{w}_W}^{n+1,v+1} \\ &+ \left.\frac{\partial R_{\mathtt{w}_P}}{\partial S_{\mathtt{w}_P}}\right|^{n+1,v} \delta S_{\mathtt{w}_P}^{n+1,v+1} \\ &+ \left.\frac{\partial R_{\mathtt{w}_P}}{\partial S_{\mathtt{w}_E}}\right|^{n+1,v} \delta S_{\mathtt{w}_E}^{n+1,v+1} \\ &+ \left.\frac{\partial R_{\mathtt{w}_P}}{\partial S_{\mathtt{w}_S}}\right|^{n+1,v} \delta S_{\mathtt{w}_S}^{n+1,v+1} \\ &+ \left.\frac{\partial R_{\mathtt{w}_P}}{\partial S_{\mathtt{w}_B}}\right|^{n+1,v} \delta S_{\mathtt{w}_B}^{n+1,v+1} \end{aligned} \tag{61}$$

where

$$R_{\mathtt{w}_P}^{n+1,v} = -T_{\mathtt{w}z_a}^{n+1,v}\Delta\Phi_{\mathtt{w}z_A}^{n+1,v} - T_{\mathtt{w}y_n}^{n+1,v}\Delta\Phi_{\mathtt{w}y_N}^{n+1,v}$$

$$- T_{\mathtt{w}x_w}^{n+1,v}\Delta\Phi_{\mathtt{w}x_W}^{n+1,v} - T_{\mathtt{w}x_e}^{n+1,v}\Delta\Phi_{\mathtt{w}x_E}^{n+1,v}$$

$$- T_{\mathtt{w}y_s}^{n+1,v}\Delta\Phi_{\mathtt{w}y_S}^{n+1,v} - T_{\mathtt{w}z_b}^{n+1,v}\Delta\Phi_{\mathtt{w}z_B}^{n+1,v}$$

$$+ C_{\mathtt{w}p}(p_{\mathtt{g}_P}^{n+1,v} - p_{\mathtt{g}_P}^{n}) + C_{\mathtt{w}s}(S_{\mathtt{w}_P}^{n+1,v} - S_{\mathtt{w}_P}^{n})$$

$$- q_{sc\mathtt{w}_P}^{n+1,v} \tag{62}$$

and, for example,

$$\Delta\Phi_{\mathtt{w}z_A}^{n+1,v} \equiv \left(p_{\mathtt{w}_A}^{n+1,v+1} - p_{\mathtt{w}_P}^{n+1,v+1}\right) - \left(p_{c_A}^{n+1,v} - p_{c_P}^{n+1,v}\right)$$

$$- \lambda_{\mathtt{g}_a}^{n+1,v}\left(z_A - z_P\right), \tag{63}$$

with similar definitions employed for the other terms [13].

The derivatives of the residuals with respect to saturation are obtained consistently with those that can be obtained by the Newton-Raphson method. The implicit calculation of the pressure field in the porous medium is performed in a first step, followed by an equally implicit calculation of the saturation field, using a fully implicit linearization.

This iterative process is conducted until convergence is achieved, following the established criteria. The systems of algebraic equations are solved by applying the Biconjugate Gradient Stabilized method using the ILU-type preconditioner [13].

4 Numerical Results

In this work, simulations were carried out considering: Darcy-type flow (Case 1); non-Darcy-type flow with the Klinkenberg effect and correction due to effective stress (Case 2); non-Darcy-type flow with the Klinkenberg effect (Case 3); and non-Darcy-type flow with correction due to effective stress (Case 4).

For the simulations, a basic set of parameters was defined, based on those used by [13] for the study of water-gas flow in a conventional reservoir with production via a vertical well. The parameters necessary for including slippage and effective stress effects were chosen after research in works dedicated to the study of unconventional low-permeability reservoirs, as was done for the horizontal well configuration.

The general parameters for the standard case, including fluid and rock properties and the geometric characteristics of the reservoir, can be found in Table 1. In this table, g_{cap} is the location of the bottom of the gas cap, measured from the top of the reservoir.

For a mesh refinement study, four distinct computational meshes were employed to determine the most suitable one and to verify the numerical convergence of the method [11]. The mesh was refined along all three spatial directions, and the physical characteristics of the porous medium and the operational conditions defined in the reference case were preserved. This study is essential for reducing errors associated with discretization and for ensuring the accuracy of the results. Table 2 contains, for the computational grids employed, the respective numbers of volumes in the x, y, and z directions, denoted as n_x, n_y, and n_z.

Figures 3 and 4 show the results of this evaluation for Case 2, displaying the gas flow rate and cumulative production curves for each configuration. As the meshes are refined, the flow rate and cumulative production curves become increasingly close to each other, with the exception of the initial region. It should be noted that the adopted well-reservoir coupling technique [20] has an artifact called numerical storage, which appears as plateaus when simulations are performed for a prescribed flow rate and when studying plots of wellbore pressure as function of time, with the time axis on a logarithmic scale. Thus, the results obtained here for the initial periods are under the influence of this artifact, which is reduced by mesh refinement and is dependent on fluid properties, rock properties, and geometry [10].

Table 1 General parameters.

Parameter	Value	Unit
b	1,000	psi
B_w^0	1.022	–
c_ϕ	4×10^{-6}	psi^{-1}
c_w	1×10^{-5}	psi^{-1}
g_{cap}	90	ft
k_0	1×10^{-7}	Darcy
$k_{rw_{max}}$	0.4	–
$k_{rg_{max}}$	0.9	–
$L_x = L_y$	1,000	ft
L_z	180	ft
L_w	500	ft
p_{sc}	14.696	psi
p_{wf}	2,000	psi
$p_0 = p^0$	4×10^3	psi
r_{wf}	0.1875	ft
$S_{g\mathtt{w}}$	0.15	–
$S_{\mathtt{w}0}$	0.20	–
T	609.67	R
T_{sc}	519.67	R
γ	1×10^{-4}	psi^{-1}
ϕ_0	0.07	–

Table 2 Meshes.

Mesh	n_x	n_y	n_z
1	64	65	22
2	128	129	42
3	256	257	82
4	512	513	162

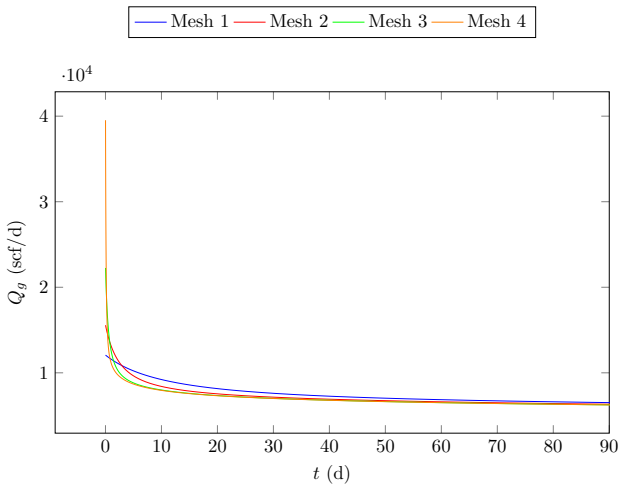

Figure 3: Mesh refinement (Case 2): gas flow rate.

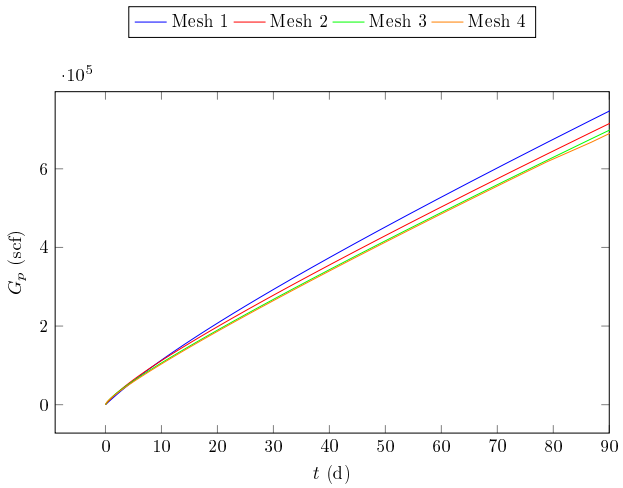

Figure 4: Mesh refinement (Case 2): cumulative gas production.

The comparison of the results revealed that Mesh 3 offers a suitable balance between accuracy and computational cost. This choice was substantiated by the overlap of the curves obtained for the more refined meshes (Mesh 3 and Mesh 4), indicating that the results obtained with Mesh 3 are satisfactory. Furthermore, the utilization of Mesh 3 leads to a reduction in simulation time compared to Mesh 4, rendering it the most effective choice for this study. Consequently, Mesh 3 was employed as the standard mesh in subsequent simulations.

Figures 5 and 6 present a comparison between the flow rate and the cumulative gas production for Cases 1 and 2 over time. In Case 1, only the flow governed by the classical Darcy's Law is considered, whereas Case 2 includes the effects of gas slippage and permeability correction due to effective stress variation.

This comparison allows for the evaluation of how these phenomena influence two-phase flow in low-permeability reservoirs. The results demonstrated that, in Case 2, the gas flow rate is higher compared to Case 1, leading to greater cumulative production over time. This behavior is primarily attributed to the Klinkenberg effect, which elevates the apparent permeability in low-pressure regions, facilitating gas flow through the rock micropores. Conversely, the correction resulting from rock deformation has an opposing effect, decreasing the effective permeability as the reservoir pressure declines. This is caused by the redistribution of mechanical stress, which results in a reduction of the gas transport capacity within the pores, with a consequent drop in reservoir pressure. Nevertheless, the combination of these two effects shows that the positive impact of gas slippage largely compensates for the negative impact of the stress-dependent correction, resulting in an overall superior performance in Case 2 in terms of both gas flow rate and cumulative production.

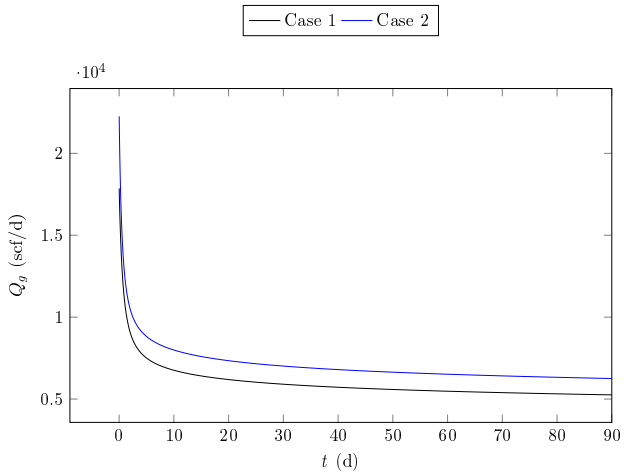

Figure 5: Comparison between Darcy and Non-Darcy cases (including all effects): gas flow rate.

The variation of gas flow rate over time is illustrated in Figure 7, while Figure 8 presents the cumulative gas production, in a comparative analysis of results obtained for Cases 1, 2, 3, and 4. In Case 3, a significant increase in gas flow rate is observed compared to the other cases, exhibiting the highest production. This is attributed to the higher apparent permeability values characteristic of low-permeability gas reservoirs when the Klinkenberg effect is influential. This increase in flow rate directly reflects the enhanced cumulative production. Conversely, Case 4 shows a significant reduction in both flow rate and cumulative production due to the stress-dependent correction effect, which diminishes the transport capacity within the pores resulting from reservoir pressure decline. Thus, the adverse impact of this effect in low-permeability reservoirs is evident.

Referring again to Figures 7 and 8, Case 2, which incorporates all considered effects, exhibits the second highest gas flow rate and cumulative production. Despite the detrimental influence of stress-dependent per-

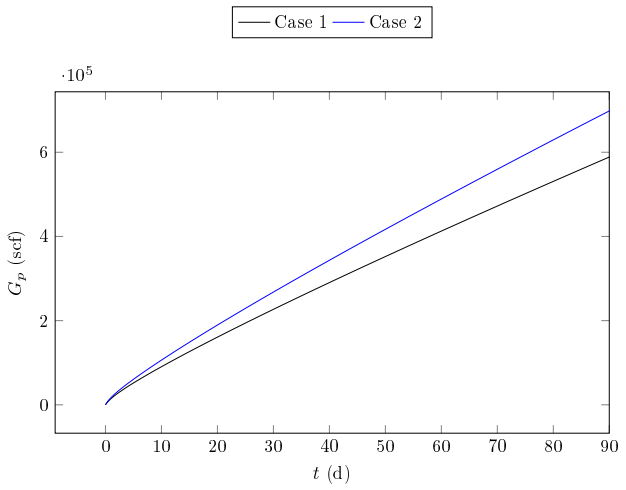

Figure 6: Comparison between Darcy and Non-Darcy cases (including all effects): cumulative gas production.

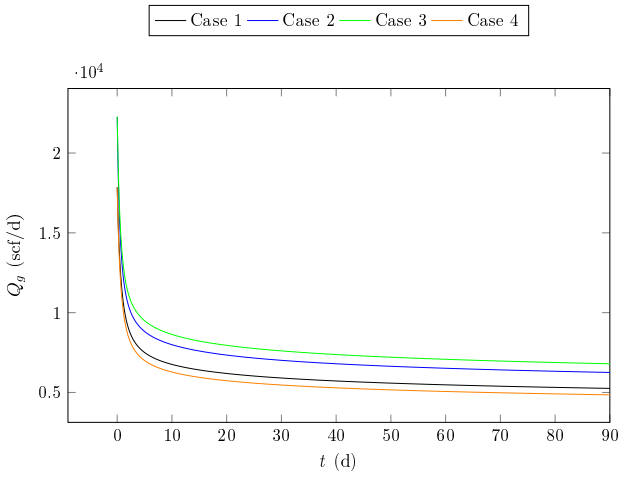

Figure 7: Comparison of all cases: gas flow rate.

meability reduction, the beneficial impact of gas slippage largely counteracts this decrease. Consequently, with respect to both flow rate and cumulative production, Case 2 is surpassed only by Case 3, where this negative stress-dependent impact is absent.

Figures 9 and 10 illustrate the impact of the Klinkenberg effect on gas production across three scenarios: b=0 psi (Darcy flow), b=500 psi (moderate slippage), and b=1,000 psi (base case). The values of this parameter reflect the magnitude of gas slippage's influence within the reservoir, directly affecting the apparent permeability. When b=0 psi, mass flow occurs without slippage, resulting in the lowest gas flow rate and cumulative production among the analyzed scenarios.

Further examining Figures 9 and 10, the scenario with b=500 psi demonstrates a moderate Klinkenberg effect across the evaluated cases, resulting in an apparent permeability that exceeds that observed in Darcy flow. A noticeable increase in gas flow rate is observed, with the

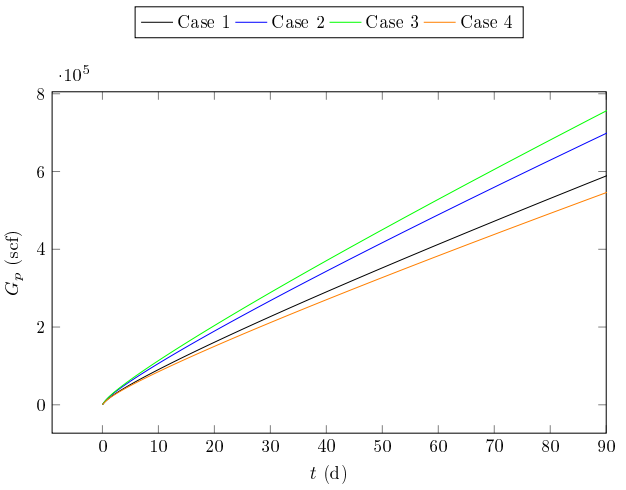

Figure 8: Comparison of all cases: cumulative gas production.

slippage effect being more pronounced in regions of lower pressure (near the wellbore). Consequently, the cumulative production experiences a significant enhancement over time, highlighting the positive impact of slippage on improving production efficiency under low-pressure conditions. Finally, for b=1,000 psi (base case), a greater intensity of the slippage effect is present, causing the most substantial increase in apparent permeability. This condition further enhances gas transport and, consequently, leads to the highest gas flow rate and cumulative production over time.

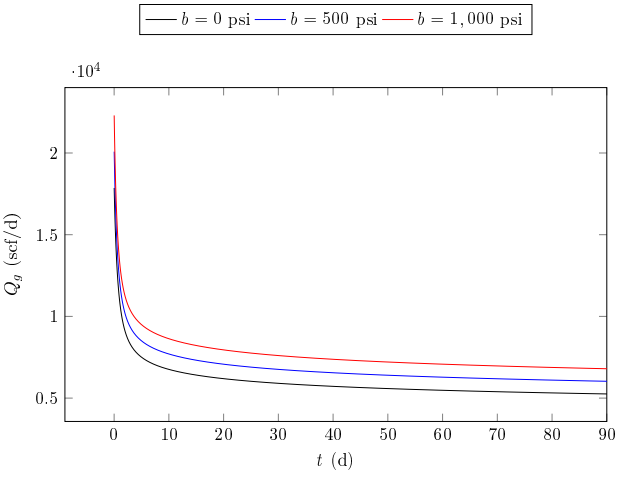

Figure 9: Impact of b variation on the Klinkenberg effect: gas flow rate.

The impact of the coefficient γ, present in Equation (3), on gas flow rate and cumulative production is illustrated in Figures 11 and 12, respectively. This coefficient influences the stress-induced changes in the matrix permeability values. For γ=0 psi^{-1}, the case of flow governed by the original Darcy's Law is observed. With no compaction of the porous matrix, the absolute perme-

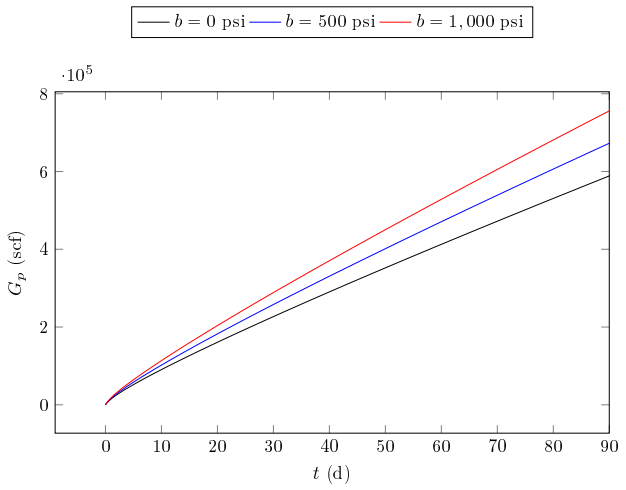

Figure 10: Impact of b variation on the Klinkenberg effect: cumulative gas production.

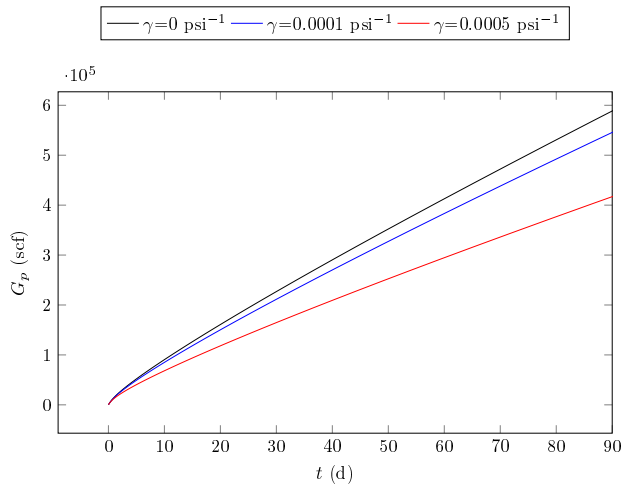

Figure 12: Influence of γ on the stress-induced deformation effect: cumulative gas production.

ability remains constant over time, irrespective of the reservoir pressure. A higher gas flow rate and cumulative production are observed, as there is no reduction in the transport capacity through the pores due to rock compaction.

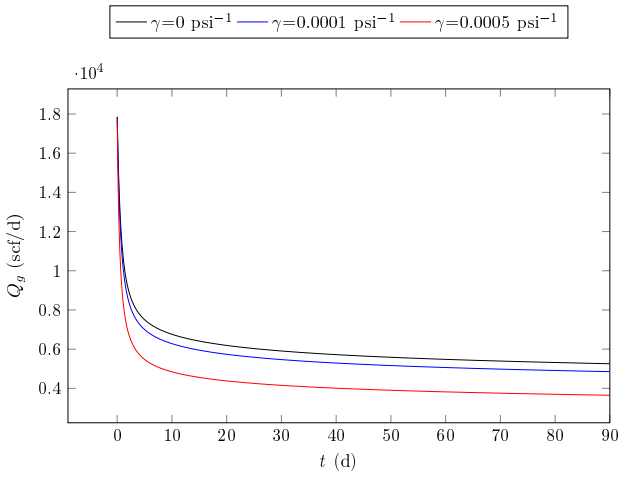

Figure 11: Influence of γ on the stress-induced deformation effect: gas flow rate.

As γ increases, the negative effects of matrix compaction become more pronounced. For the reference case (γ=0.0001 psi^{-1}), a moderate reduction in absolute permeability occurs, resulting in a comparatively small decrease in gas flow rate and cumulative production. However, for γ=0.0005 psi^{-1}, the effects of compaction intensify, leading to a significant reduction in apparent permeability and consequently a sharp decline in gas flow rate and substantially lower cumulative production.

Moving on, the impact of horizontal well length was investigated, with the results presented in Figures 13 and 14. For L_w=400 ft, the limited contact area considerably reduces the capacity of fluids to flow from the rock to the wellbore. Consequently, the gas flow rate is lower, directly reflecting a reduced cumulative production. In the base case, L_w=500 ft, an improvement in both gas flow rate and cumulative production is observed. The increased well length allows for a larger contact area with the matrix, enhancing the drainage of gas present in nearby productive zones. Thus, it is evident that the utilization of longer horizontal wells enhances operational effectiveness in low-permeability reservoirs. When L_w=600 ft, the well reaches its maximum length for the tested cases. Its greater extent enables even more effective drainage, leading to the highest gas flow rate and cumulative production among the evaluated scenarios.

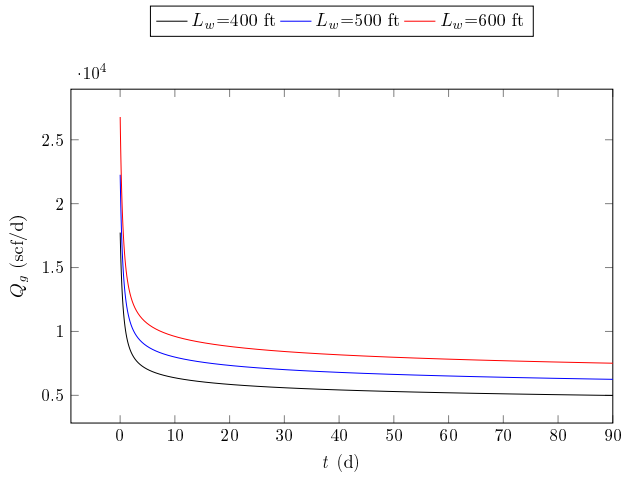

Figure 13: Effect of horizontal well length variation (Case 2): gas flow rate.

The gas flow rate and cumulative production curves for varying porosity values (ϕ=0.05, 0.07 (reference

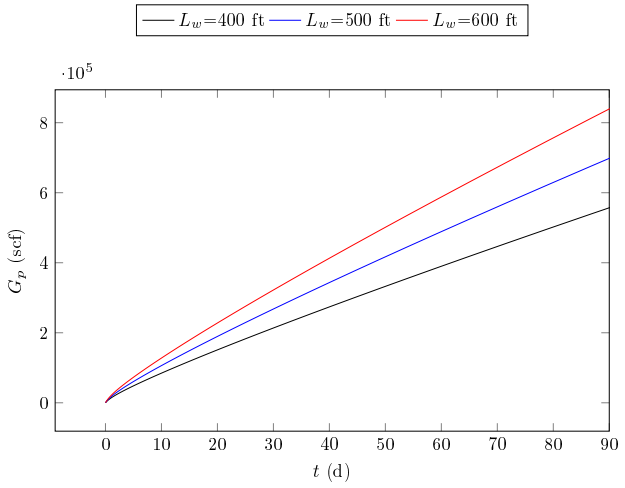

Figure 14: Effect of horizontal well length variation (Case 2): cumulative gas production.

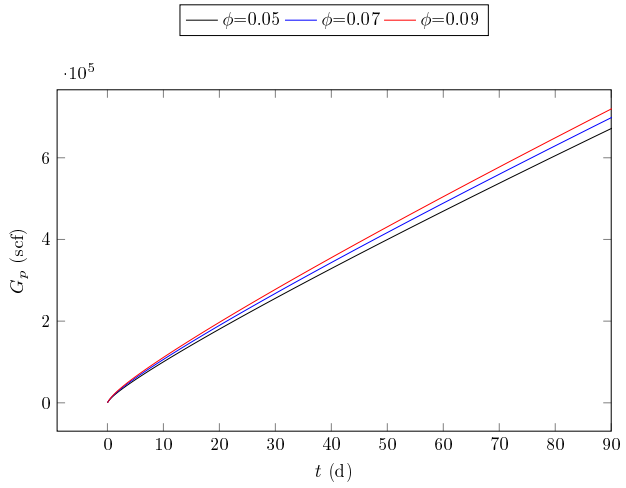

Figure 16: Impact of porosity variation (Case 2): cumulative gas production.

case), and 0.09) are presented in Figures 15 and 16, respectively. It is evident that increasing porosity leads to a higher gas flow rate, as both the storage capacity and transport capability of the gas are directly influenced by this property. A greater porosity value corresponds to a larger volume of gas available for flow.

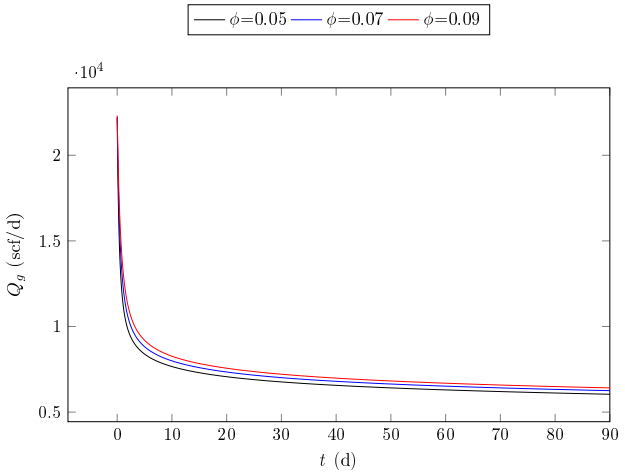

Figure 15: Impact of porosity variation (Case 2): gas flow rate.

For ϕ=0.05, the flow rate is the lowest due to the reduced storage capacity of the reservoir. In the intermediate case (ϕ=0.07), an increase in flow rate is observed, demonstrating the positive impact of enhanced porosity. Finally, for ϕ=0.09, the flow rate is the highest, being more pronounced in the initial stages and gradually declining over time. The cumulative gas production follows the same trend observed for the flow rate. The highest porosity (ϕ=0.09) results in superior cumulative production, owing to the larger volume of gas stored and available for production. Over time, the difference between the cases becomes more distinct, as the greater storage capacity allows for more sustained production. Conversely, with ϕ=0.05, the cumulative production is the lowest, limited by the smaller gas volume present in the reservoir. Regarding ϕ=0.07, an intermediate cumulative production is observed.

Figures 17 and 18 present the analysis of absolute permeability (k_0) for gas flow rate and cumulative production, respectively, considering three permeability values.

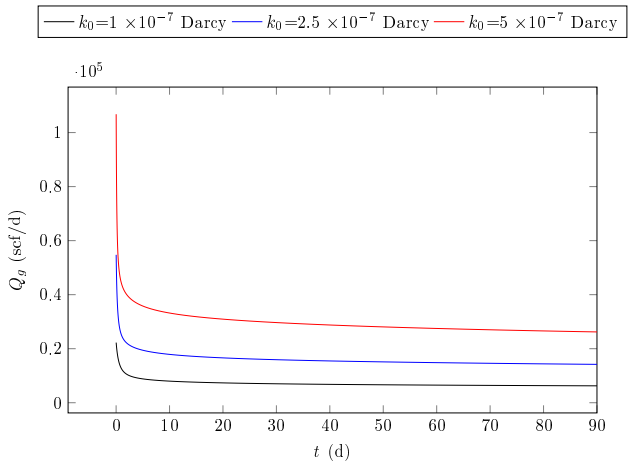

Figure 17: Impact of absolute permeability variation on production (Case 2): gas flow rate.

As the absolute permeability value increases, the initial and final values of both flow rate and cumulative production also increase. For k_0=5 $\times 10^{-7}$ Darcy, the initial flow rate is higher, and the decline is slower over time, whereas for k_0= 1 $\times 10^{-7}$ Darcy, it is the lowest, indicating greater resistance to gas flow within the reservoir. The cumulative volume produced exhibits similar behavior, as the increase in permeability results in its faster

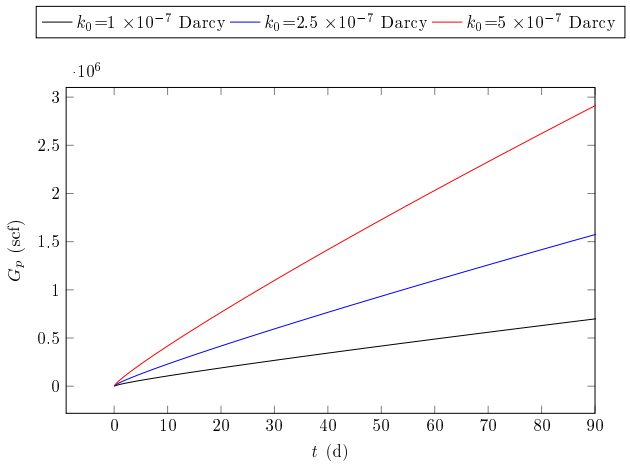

Figure 18: Impact of absolute permeability variation on production (Case 2): cumulative gas production.

growth due to the enhanced ease of fluid flow within the porous medium as a consequence of its increase.

5 Conclusion

This work presented numerical simulations aimed at investigating production in low-permeability natural gas reservoirs under two-phase water-gas flow, considering the effects of gas slippage and permeability correction due to effective stress variation. The formulation, based on the Picard-Newton method, successfully captured the typical curves for gas flow rate and cumulative production. It is understood that a quantitative evaluation necessitates a comparison with other results derived from different numerical simulators, experimental data, or analytical solutions for specific cases. Increasing the coefficient b resulted in an enhancement of apparent permeability, demonstrating its relevance in low-permeability reservoirs. Consequently, increases in gas flow rates and cumulative production were observed.

Elevating the modulus γ intensified the effects of porous matrix compaction, leading to a decrease in permeability and consequently restricting gas mass flow and negatively impacting cumulative production. As its values were increased, the apparent permeability reduction became more pronounced with declining reservoir pressure. Enhancing porosity exhibited a direct correlation with increased gas flow rate and cumulative production. Higher porosity values lead to a greater gas storage capacity within the reservoir, resulting in improved recovery over time. Regarding the transport capacity through the porous medium, the effect of increasing porosity values is the inverse of that observed with increasing absolute permeability. Concerning absolute permeability, higher values correspond to lower flow resistance. As a consequence, a higher initial flow rate and a slower decline were obtained, yielding a larger cumulative gas volume.

In low-permeability reservoirs, the limitations imposed on flow are significant, thus emphasizing the necessity of employing stimulation techniques to enhance apparent permeability and enable production. In this regard, increasing the length of the horizontal well facilitated a larger contact area with the porous matrix, implying an increase in both gas flow rate and cumulative production. Finally, this study highlights the importance of incorporating accurate models for simulating operational strategies to improve reservoir management.

References

[1] R. Agrawal and K. Zhang. Flow behavior and challenges in shale gas reservoirs. Journal of Unconventional Oil and Gas Resources, 5:47–61, 2014.

[2] R. F. Aguilera. The Economics of Unconventional Oil and Gas Resources. Springer, Berlin, Germany, 2010.

[3] N.S. Al-Mohannadi. Simulation of Horizontal Well Tests. PhD thesis, Colorado School of Mines, Golden, USA, 2004.

[4] Mohammad Al-Twaijri, Zhaohui Xia, Wei Yu, Liangchao Qu, Yunpeng Hu, Yifei Xu, and Kamy Sepehrnoori. Numerical study of complex fracture geometry effect on two-phase performance of shale-gas wells using the fast EDFM method. Journal of Petroleum Science and Engineering, 164:603–622, 2018.

[5] T. Babadagli, A. Al-Yaseri, and H. Roshan. Physics of fracturing fluid interaction with unconventional reservoirs: Formation damage or enhancement? Journal of Unconventional Oil and Gas Resources, 11:107–121, 2015.

[6] T. Barth, R. Herbin, and M. Ohlberger. Finite Volume Methods: Foundation and Analysis. In E. Stein, R. Borst, and T. J. R. Hughes, editors, Encyclopedia of Computational Mechanics. John Wiley & Sons, Inc, New Jersey, USA, 2 edition, 2017.

[7] Z. Chen, G. Huan, and Y. Ma. Computational Methods for Multiphase Flows in Porous Media. Society of Industrial and Applied Mathematics, Philadelphia, USA, 2006.

[8] C. L. Cipolla, E. Lolon, M. J. Mayerhofer, and N. R. Warpinski. The relationship between fracture complexity, reservoir properties, and fracture-treatment design. SPE Production & Operations, 24(4):575–592, 2009.

[9] J. G. S. Debossam, J. D. S. Heringer, G. Souza, and H. P. A. Souto. Numerical simulation of single-phase flow in naturally fractured oil reservoirs. Coupled Systems Mechanics, 8(2):129–146, 2019.

[10] J. D. dos Santos Heringer, G. de Souza, and H. P. Amaral Souto. On the numerical simulation of non-isothermal heavy oil flow using horizontal wells and horizontal heaters. Brazilian Journal of Chemical Engineering, 41:179–196, 2024.

[11] T. Ertekin, J. H. Abou-Kassem, and G. R. King. Basic Applied Reservoir Simulation. SPE Textbook Series 7. Society of Petroleum Engineers, Richardson, USA, 2001.

[12] N. Ezekwe. Petroleum Reservoir Engineering Practice. Prentice Hall, Westford, USA, 2010.

[13] M. M. Freitas, G. Souza, and H. P. Amaral Souto. A Picard-Newton approach for simulating two-phase flow in petroleum reservoirs. International Journal of Advanced Engineering Research and Science, 7(4):428–457, 2020.

[14] D. Gao and Others. Impact of stress-sensitive permeability on gas production in shale reservoirs. Journal of Natural Gas Science and Engineering, 15:55–67, 2013.

[15] Yong He, Jianjun Wang, Xiaoqing Huang, Yue Du, Xiang Li, Wenshu Zha, and Daolun Li. Investigation of low water recovery based on gas-water two-phase low-velocity non-Darcy flow model for hydraulically fractured horizontal wells in shale. Petroleum, 9(3):364–372, 2023.

[16] J. D. S. Heringer, J. G. S. Debossam, G. Souza, and H. P. A. Souto. Numerical simulation of non-isothermal flow in oil reservoirs using two-equation model. Coupled Systems Mechanics, 8(2):147–168, 2019.

[17] S. A. Holditch. Tight gas sands. Journal of Petroleum Technology, 58(6):86–95, 2006.

[18] L. J. Klinkenberg. The permeability of porous media to liquids and gases. Drilling and Production Practice, American Petroleum Inst., 1:200–213, 1941.

[19] R. D. Mindlin. On the theory of small elastic deformations of bodies with irregular boundaries. Journal of Applied Mechanics, 28:27–32, 1961.

[20] D. W. Peaceman. Interpretation of well-block pressures in numerical reservoir simulation. Society of Petroleum Engineers Journal, 18(3):183–194, 1978.

[21] E. Shahraeeni and A. Firoozabadi. Multiphase flow in tight formations: Challenges and new perspectives. SPE Journal, 20(4):700–711, 2015.

[22] Haibin Wang and Mark D. Zoback. Permeability evolution due to dynamic changes in effective stress during depletion in shale gas reservoirs. Journal of Natural Gas Science and Engineering, 51:102–114, 2018.

[23] Yunfeng Xu, Guanglong Sheng, Hui Zhao, Yanni Hui, Yuhui Zhou, Jialing Ma, Xiang Rao, Xun Zhong, and Jie Gong. A new approach for gas-water flow simulation in multi-fractured horizontal wells of shale gas reservoirs. Journal of Petroleum Science and Engineering, 199:108292, 2021.

[24] Rui-Han Zhang, Lie-Hui Zhang, Hui-Ying Tang, Sheng-Nan Chen, Yu-Long Zhao, Jian-Fa Wu, and Ke-Ren Wang. A simulator for production prediction of multistage fractured horizontal well in shale gas reservoir considering complex fracture geometry. Journal of Natural Gas Science and Engineering, 67:14–29, 2019.

[25] Yunhao Zhang and Daoyong Yang. Modeling two-phase flow behaviour in a shale gas reservoir with complex fracture networks and flow dynamics. Gas Science and Engineering, 119:205112, 2023.

Towards Volumetric Brazilian Geography

The *Geomer* as a Useful Particulate Region

Richard B. Cathcart
GEOGRAPHOS, Burbank, California, USA
rbcathcart@gmail.com

Nilo Serpa
L'Académie de Bordeaux; *L'Académie de Paris*; Centro Universitário ICESP, Brasília; Universidade Santa Úrsula, Rio de Janeiro

Received: _20 May 2025_/ Accepted: _08 Jun 2025_ / Published: _11 Aug 2025_.

Abstract: Any application of down-to-earth Macro-Imagineering may result in speculative infrastructures, instrumented, and strategically installed at appropriate places within our Earth's cherished bioshell. The article expounds, from an open-minded Macro-Imagineering viewpoint centered specifically on Brasil, avoiding the pervasive and explanatorily superfluous "global warming" notion, on several budding futuristic techno-social approaches to our already anthropocentric [1-2], and increasingly unitary planet. It was stimulated by Brazilian quantum physicist Nilo Sylvio Costa Serpa's indicative, inspired scientific terminology: "Quantum-Imagineering" [3]. With that instigative 2019 statement in CALIBRE, it is to be hoped another useful investigative and explicative thread for academic-level taught Geography in Brasil, after Josue de Castro [(1908-1973) 4], can be commenced at once. In effect, a new "school" of Academic Geography may become established.

Keywords: Macro-Imagineering, Dosmozoicum, Geomer, Hans Carol, Social media falsehoods, Anthropogenic global warming, Quantum computation, Brazil, Guanabara Bay, Mining.

Resumo: Qualquer aplicação especulativa, porém, realista de *Macro-Imagineering* pode resultar em infraestruturas instrumentadas e estrategicamente instaladas em locais apropriados dentro da preciosa *bioshell* da Terra. O presente artigo expõe, a partir de uma perspectiva aberta de *Macro-Imagineering* centrada especificamente no Brasil, e, evitando a noção generalizada e quase supérflua de "aquecimento global", diversas abordagens tecnossociais futuristas em desenvolvimento para o nosso tão antropocêntrico [1-2] e cada vez mais unitário planeta. Foi estimulado pela terminologia científica indicativa e inspirada do físico quântico brasileiro Nilo Sylvio Costa Serpa: "Quantum-Imagineering" [3]. Com essa instigante declaração de 2019 na CALIBRE, espera-se que outra linha investigativa útil e explicativa para o ensino acadêmico de Geografia no Brasil, após Josué de Castro [(1908-1973) 4], possa ser iniciada de imediato. Com efeito, uma nova "escola" de Geografia Acadêmica pode ser estabelecida.

Palavras-chave: *Macro-Imagineering*, *Dosmozoicum*, *Geomer*, Hans Carol, Falsidades nas mídias sociais, Aquecimento global antropogênico, Computação quântica, Brasil, Baía de Guanabara, Mineração.

Dedication: to the memory of Alexander A. Bolonkin (1933-2020).

1. Introduction

Many of the too-vociferous personalities and famous organized groups usually identified by world-spanning electronic and print social media as “climate scientists”, as in the usual “climate scientists say…” storyline titles, have until recently actually been Flat Earth climate modelers! (“Climate Activists” mostly parrot the storylines spouted by acclaimed “climate scientists” to advance ever-more elaborated social macro-engineering schemes of so-called worldwide Crisis Management. It would seem, then, that the conveniently-adopted ersatz conventional “climate science” is today intensely focused on social media-ghettoizing its barely organized opposition, Brazil’s alleged “Deniers” as well as groups elsewhere) [5]. With uncommon candor, several honest scientists have recently unveiled an important global climate-modeling super-computing programming discrepancy: “A mostly forgotten assumption in climate models is that of a flat Earth atmosphere. Spherical atmospheres intercept 2.5 W-m^2 more sunlight and heat the climate by an additional 1.5 W-m^2 globally” [6]. In other words, all the expensive digitized super-computer read-outs and fanciful graphics, focused almost exclusively on humankind’s past carbon dioxide gas emissions, generated so far have ignored the basic fact, known from real-world Portuguese experience since the first circumnavigation of our planet hundreds of years ago, of Earth’s sphericity as well as its true placement in universal time-space! The monologues about the present-day Earth’s global and regional climate, whatever that may be in reality [7], has become a corrupted, hyperbolic popular social media topic of verbose governmental polities, intricate verbal publicized discussions (employing intentionally arcane and misleading jargon) about alleged public-policy benefits that are, relentlessly, neverendingly purveyed — nay, inflicted to the point nowadays of inducing pseudo-deafness, on too-attentive courteous Brazilian laypersons.

Since at least the mid-1960s, once normal everyday human environmental concerns — survival and increasing personal future prosperity — have been effectively shaped by elaborate but unperfected super-computer model projections of, mostly, worldwide climate regime catastrophes. From the very start of this over-arching documentation effort, the effort was outrageously irrelevant; because of the undeniable absence of reliable, long-term real-world scientific measurements from well-kept, placed, and operated weather instrumentation it only amounted generally to wasted taxpayer funding! It was a bandwagon fueled by besieged taxpayer monies, quickly boarded by those opportunists mostly intent on prolonged, well-paid careers in a vaporous “climate forecasting science” campaign that, gradually, morphed into the even more lucrative Social Engineering of Brazilians as well as other humans; briefly summarized, thundering herds of so-called “climate scientists” groomed themselves as “heroes” and, sometimes, portray themselves in popular social media as comfortably living and still working “social justice” martyrs. Such persons are not truly “bad” people, merely “scientific fashionists”, opportunistic persons who have foolishly adopted weak intellectual frameworks as hypothecators and theoreticians. None of these posing persons are another Josue de Castro. However, aware that we must earn a living and that we are virtuously anti-Big Corporations, at least in our public political stance, we now seek generous public-funding of a total-solution macro-project that could, in an instant, counter the anthropogenic as well as actual natural Global Warming of Earth’s air: pay us well to increase our planet’s gravity! Because air contains vaporous freshwater (a dilute condensable) known to be radiatively active, if Earth’s gravity [8] were somehow increased—perhaps by adding extra-terrestrial mass obtained from other parts of this Solar System—the total path length of the aerial freshwater droplets will be decreased, leading inevitably to significant reduction of our planet’s so-called Anthropogenic Greenhouse Gas Emissions Effect! (Symmetry is our primary yearning.)

Generally, most people want accurate information/data about their region’s weather, not gasping at fugitive ethereal and useless speculations about their whole planet’s air condition, globally or regionally. The innumerable warnings issued by self-described “experts” has become a Brazilian life-style improvement-hindering cacophonous chorus of nonsensical crisis constructions totally without

reference or true meaning to any Brazilian's real-world life-style preferences or on-going healthful active lives which do require some feasible 21st Century safety and comfort advancements. (For example, see the 2024 Brazil-recorded movie ***Ainda Estou Aqui*** or, in English, ***I'm Still Here***, the true story of Eunice Paiva's survival after her dissident engineer-politician husband, Rubens Paiva, disappeared, by force of government.) Numerous such reported climate-data projections have only served those of a certain pecuniary persuasion — persons and organizations that have permitted themselves to be overwhelmed by airy hyperbolized hypotheses and mathematized gibberish but who cash corpulent pay-checks and enjoy, prospectively, very high retirement Brazilian Real and centavos perks. In fact, the impressive government and academia-housed electronic gadgetry (bought by law-enforced mandatory taxpayer contribution), along with its blabbering, publicity-seeking white-coated laboratory supercomputer modelers and their associated press-release penners, seems to thoroughly stunt the normal macro-imaginations of all who partake of its addictive drug-like social news miasma of mapped globalized and impending future disasters.

In short, "Climate Science", massaged and media-emitted by excessively fictionalized — after all, they really speak only of our "future"— social media pronouncements, remains ersatz Science stultified and sullied, shifted to an inconsequential real-world status in terms of actually learning something factually new about our macro-problem beset planet of ecosystem-nations and our entire world's actual functions. With politically strategic and tactical duress, boldly implied — not merely inferred by "Deniers" — their socially hostile wannabe intellectual masters in government and academia, yet four-dimensional thinking is still done by good persons due to, not so extraordinarily, some considerable effort of self-control as well as morality, willfulness and ethicalness, uncorrupted by erroneous flat-Earth programmatic assumptions foisted for unselective consumption by 2025 AD "climate science modelers" and their political and financial power-holding directors.

After mining at least 58,000 square kilometers of Earth's landscape [9], human civilization has reportedly constructed >150,000,000,000 m^2 of air-conditioned structures; fewer and fewer urbanized Brasilian taxpayers are outdoors more than 10% of their day. More air-conditioned structures are being built everywhere humans stay for extended periods of time. Exception for a few extant spaceships and some laboratory experimental pressure chambers, no natural geographical place exists anywhere that allows a perfect demarcation of indoor and outdoor environments, and especially so since the advent of mechanical ventilation during the 19th and 20th Centuries [10]. Described differently, because of humankind's technical progress, people everywhere are becoming less and less concerned by ambient regional weather regimes, whether normal or occasionally extreme in variation, and certainly of super-duper computed and scarily-advertised impending falsely futuristic Earthly climate change. The "Final Version" of the Sixth IPCC assessment report (AR6), illustrates large increases in Global Warming over those alarmist documents issued previously. Essentially, their technically and intellectually imperfect and monetarily-costly work-product, conceived and executed *after* the usual unreported Battle of Committee memberships, became one meant to predict peoples' actions founded on dramatic post-issuance notions — that is, the IPCC goal, taken from its supposedly authoritative reports on global climate's state, instructed the world-public what it ought to be and what, collectively, it should do in the real-world to ameliorate their previous misbehaviors. In other words, a continuance of falsehood-plagued "Climate Science" must be permitted resulting in a perpetuation of our tax-tormented civilization! The champagne-cork poppers at the Sixth IPCC report's presentation, with every enjoyable bottle of that delicious bubbly uncorked, release once securely-sequestered life-threatening carbon dioxide gas [11]. Most criminals usually reject the concept of "shame", don't they?

How may non-"Climate Science" persons escape the omniscient bureaucratic glare, the crass and coercive behavioral influence of those diktat-issuing self-proclaimed "experts"? We suggest that quite soon, possibly during 2025 even, individuals will be capable, with the help of artificial intelligence

empowerments and super-computer miniaturization, of modeling their own daily weather forecasts as well as, if they so choose, to model interesting future global and regional Earth climate regimes, possibly as pure family-entertainment. Microsoft's 2025-announced invention of Majorana-1, a quantum processing unit powered by a topological core designed to scale to a million q-bits on a single computer chip indicates the trend in future commercial computer operations! Most collected data need to be spatially referenced. For example, developed technology already allows open-data monitoring and prediction of local weather using TEMPEST, a commercial AI-assisted personal meteorological event-reporting system currently sold by Weatherflow. Because of the existence of the World Wide Web, the day should come — soon — when people will not any longer require for their survival and prosperity the flawed predictive work-products issued (at some significant taxpayer cost) to them by politicized climate prognosticators employed by tax-bloated governments and rogue major organizations. Fortunately, since the 1960s, it has become a given that the event-process of gathering and analyzing/synthesizing data about our Earthly surroundings is becoming exceptionally inexpensive; the extant miniaturized computers of AD 2025 make possible the materialization of reporting sensors in every objective *thing* manufactured or retro-fitted and many of those features and creatures we still habitually mention as being strictly Nature are bugged! Individual home- or work-based Brazilian "Deniers" can crowd-source future variously scaled geographical climate predictions which also may serve as family entertainment, electricized group fun, during hot summertime evenings or cold wintertime days! Even the Amazon River Basin's inhabitants, plants, and animals as well as humans must cope with occasionally "cold spells" caused by infrequent cold air-mass intrusions from the far South!

"Schools" of Geography — that is, a shared like-mindedness of theoretical spatial outlook that appears to be somewhat traditional — pervades (as elsewhere) Brasil's Academia. Of course, such shared opinion goes beyond a mere historical view on geographical thought, geosophy, as propounded in the USA during 1947 by John Kirtland Wright (1891-1969). Bruno Carvalho, in his presentation "After the Future: Scales of Belonging in the Urban Anthropocene" given before the 3-4 October 2019 "Future of Geography Conference" held at Weatherhead Center for International Affairs, Harvard University, exampled Roberto Burle Marx as belonging to a "school" focused on urban infrastructure. However, the Brazilian geographer Milton Santos (1926-2001) has also been impressively lauded as the founder of a true "school" of theoretical geographical exposition in Brasil [12-13]. Brasil is the only ecosystem-nation in the New World whose population communicates using the language of Portugal, a *geomer* of the Old World; so, whether we are concerned by the viewpoints on theoretical urban and rural infrastructures of the *cariocas* or the *paulistas*, the means of sharing directly is an ancient and noble language! Admittedly, this essay is quasi-polemical and ought to be read in that spirit. Here, however vainly, the reader is being enticed to adopt a theoretical opinion on developing technologies as these are taking place in the discipline and which may efficiently allow its adopters to relate to the vocation of Geography and of infrastructural progressiveness for Brasil. When will the time arrive, probably sometime after 2025 AD, when exa-scale super-computations will be done anywhere in Latin America [14].

Since our shared present-day Earthly environmental trend conditions and object shapes result from Homo sapiens' [15] outlook and Nature's past imperfect infrastructural accomplishments, Brazilian futures are, therefore, going to be a unique result of humans' regionalized species realized and unrealized scientific and other equally vivid environmental dreams based on ever-changing verified knowledge about Nature commonly implemented by practical constructive and destructive predictive efficacy. We have noted the intriguing illusional cover-art of a 2018 Spanish textbook, ***Antropoceno: La politica en la era humana*** (Taurus: Madrid) by Manuel Arias-Maldonado which focused on a plastic bag floating in seawater that, at first apprehension, seemed to be a free-floating, orphaned iceberg. Such propagandized icebergs nowadays are often perceived by many Earthlings as truly symptomatic of a drastic effect, purely anthropogenic, of Global Warming; instead, we immediately envisioned the current pollution of Guanabara Bay next to Rio de Janeiro, Brazil, by unsightly floating plastic trash! This article attempts, in

a small way, to advance academic Geography, especially as practiced in modern-day Brasil, to a different organizational state reflected in the further practical development of. Hans Carol's region segregation theory which can be finalized in the reasonable time-space concept of his *geomer* conceptualization, becoming a regionalization technique applicable to any celestial body as well as universal time-space within our known and mysterious Universe. Stephen Salter's proposed and developing Geo-engineering technology for stratus Cloud Brightening seems to be an especially applicable example of particularization in the real-world. Even more au currant is "energy meteorology" based on individual photovoltaic panels [16]. Pixelated (digital electronics) meteorology, in effect!

Childish wannabe world-changing Geo-engineers — Salter is not ever to be construed as belonging to this class of propagandists — might chose to play an inconsequential but supposedly "rigorously scientific" board-game, ***Planet***, using rolled randomized instructive, indeed God-like, dice which was first marketed worldwide on 20 April 2019; or, they could diligently study and learn comprehensively in formalized schooling, and self-examined elsewhere experiences afterwards. A lucky few might possibly be destined to become down-to-Earth macro-imagineer trainees courageously attempting to solve our world's largest feedback and optimization control macro-problem, the careful maintenance of the intact but friable Earth-bioshell! A few years ago, a distant dear friend of several decades, residing in Israel, Joseph Friedlander, penned a fascinating technology paradigm-breaking essay on a potential ore-mining technique exceeding today's superficial bio-mining R&D efforts: "What If We Get The Ability To Extract by Nanotech Rare Elements From the Bulk of the Earth?" [17]. Therein, he macro-imagined and proposed the sub-surface ground-mass' near-term future techno-purgation, by multiple 24/7/365 ecologically landscaped and macro-engineered tree-shaped installations utilizing anthropogenic poly-metal alloy nanites with the awesome capability, by incessant subterranean tunneling, to forcefully penetrate hard and unfractured country-rock (like plant roots [18]) that can then expeditiously dissolve desirable selected minerals and pump them rapidly upwards (out of the Earth-crust into the air or a container) through nano-scale pipelines (dubbed "tendrils") to assigned dedicated end-use processing and shaping commercial factories. (Precursor tiny mining machines like those envisioned by Friedlander might first appear as floating in a fluid industrial home-ground…say, cleaning the State of Rio de Janeiro's Guanabara Bay sediment floor of its various embedded toxic particles cast away by a negligent industrial complex, artfully reclassifying such fragments as valuable, mineable "urban ores".) Techno-purgation will not leave any mine wastes—the unwanted, currently uneconomic, solid, and liquid materials usually dumped at or near mine sites and which subsequently often pose considerable risks to nearby life and landscapes when stored in poorly maintained mounds and impoundments. Too, any Earth-crust changes that are located beneath Nature's normal impress of aerial erosion remain almost permanent in terms of our planet's singular Holocene Geologic Time period [19]. The anthropocentric term "extremophile" biota — that is, forms of life coping with >1.4 kbar or completing a life-cycle in temperatures ranging from ~2^0 Celsius to ~60^0 Celsius — shall be considered herein as a boundary-marker sometimes below the known limits of wind, oceanic turbulence and running water erosion. Wisely, Joseph Friedlander foresaw the absolute need for accurate forecast-targeting of future industry-required ores: "This tendril net would give, down to the individual…(cubic) meter, a programmable access and sensor network. Now we must imagine something like vibrational tomography that would use sound, ultrasound, or other communicable pulses to listen for and 'feel' out the atoms within reach. The analysis of the data would be a new definition of Big Data, made possibly by… [special vat-confined data-processing nanites permanently situated within discrete Earth-surface facilities]." Today, both daunting macro-problems are being addressed preliminarily. So, our rather insubstantial informational storyline seems to successfully indicate the impending likelihood that Homo sapiens, including Brazilians, could quite soon perhaps live by geographically vast currently speculative ecological Earthly infrastructures; what follows are a few focused thoughts on matter and energy not ordinarily discussed by professional quantum geographers anywhere…so far!

Since our species first existed, the Earth's bioshell has been an environment functioning more and more as an objective result of imposed human macro-imagination, as typified herein by Joseph Friedlander as well as scientific and engineering information; operating technology ***is*** the final and truest test of which alleged facts of science are useful during our lifetimes as well as possibly beyond. In his noteworthy 1970 Ph.D. dissertation, ***The Great Drought: Northeast Brazil, 1877-1880***, Dr. R.L. Cunniff recounted the costly economic real-world effort effected in Brazil's *Sertão* region to counteract that region's natural climate regime drought conditions through the creation of enormous freshwater reservoirs which were correctly assumed to increase precipitation in the surround after freshwater's massive pooling. This geographical notion for deliberate human actions is indisputably geo-physically correct, but the result following implementation is financially unsatisfactory and generally insufficient to broadly increase the rainfall onto landscapes immediately adjacent to artificial reservoirs. In other words, Brazilians have previous experience with a faddish "Climate Science"-prompted Geo-engineering scheme that failed! However, what was clearly demonstrated is a volumetric approach to particularized ecosystem-nation geography [20].

2. **World alternates or inutile idealities?**

Since 20 May 2019, the basic measurement unit of all material mass, the kilogram, has been redefined by a quantum quantity, the Planck constant: nowadays a crystal-sphere of one kilogram is determined to be $2.152538397 \times 10^{25}$ atoms of silicon-28. One 70-kilogram person consists of $\sim 7 \times 10^{27}$ atoms whilst the whole Earth is comprised of $\sim 1.3 \times 10^{50}$ atoms. Thus, for each of our Earthly bioshell's presently living good or bad humans [21] — say, 7 billion moral and immoral persons in total — the planet affords, just approximately, 0.186×10^{23} atoms! Amazingly, atomic force microscopes have been employed as cinematographic instruments! The proposed chronostratigraphic unit, the "Anthropocene" has been rejected by professional geoscientists yet persists in the popular media. However, amongst scientists of many persuasions, there is a huge range of fuzzy and firm apprehensions, perceived or cloudy (sometimes imperceptible) meanings and disorganized or even unusable definitions! Since AD 1977 when the Silurian-Devonian boundary was pinned with a bronze plaque marking a Global Boundary Stratotype Section and Point, no such plaques have been located anywhere on or in the landmass or territorial off-shore seascape of South America! Radionuclides produced by atomic-bomb explosions during the twentieth-century may yet serve as the ideal marker for the start of Earth. As professionalized quantum geographers with diverse skill-sets and educational backgrounds, we find the term "Anthropocene" itself utterly redundant, more than a little anachronistic and far too politically charged to be at all useful in our everyday work-practice. In fact, the so-called stratigraphic surface that we commonly observe about us as pedestrians and vehicle-riders during the early-21st Century is merely another globalized, obviously new, *xenoconformity*, situated beneath an unknown, but nevertheless allegedly large, mass of cosmic space dust and debris as well as a rainout of fallen radioactive anthropogenic rubbish, an Earth-material geoscientific record of some profound pervasive anthropogenic alterations done to our species' only full-time celestial dwelling, the Earth [22] — but only that; some claim the Anthropocene is already evidently becoming expressed on Mars's rugged ocean-less surface by the extension of human and robotic explorations [23].

Instead, GEOGRAPHOS has usually adopted *Dosmozoicum* [24], meaning "Age of Human Life in Outer Space" as a far truer generalizing term-of-art for what is really happening to our present-day developing planetary homeland and its immediate spatial environs in this scarcely inhabited Solar System. (Indeed, "the solar basin" is the toponym for the small fraction of solar particles emitted into bound orbits, accumulating in our perceived and measured Solar System [25]; in astrophysics Earth's "sphere of influence is usually simplistically defined by Laplace's radius or Hill's radius.) The phrase "Atomic Age" was coined by the deservedly famous journalist William Leonard Laurence (1888-1977) in his 26 September 1945 ***New York Times*** front-page column "Drama of the Atomic Bomb Found Climax

in July 16 Test". That old descriptive phrase laden with historical absolute legitimacy, is surely more than sufficient to accurately designate our late-Holocene *Dosmozoicum*! Wartime and peacetime fission and fusion atomic explosions have induced radioactive fallout — indeed, Elugelab Island in the South Pacific Ocean was comminuted instantaneously by Homo sapiens' explosion of its first thermo-nuclear device on 1-2 November 1952 and, recently, radioactive anthropogenic pollution has been found by explorers in the deepest hadal depths of the world-ocean, the Mariana Trench. While recalcitrant pro-"Anthropocene" geoscientists, along with their parrot-like mass-media sycophants at this time still dominating the world news-media and politics at all appreciable levels, publicly rejoice at the prospect for perpetual use of the term "Anthropocene" and its associated terminologies and nugatory outlook — for example: "We can therefore, imagine a 'commercially dead' planet Earth as a possible end of the 'Anthropocene…period" [26] — GEOGRAPHOS asserts that the controversially and highly-topicalized evidence being advanced as a sound underpinning for an Earth/Homo sapiens "Anthropocene" epoch is non-confirmatory. The likely geological fingerprint of the audaciously presented Anthropocene, while demonstrably clear, will not differ greatly in many respects from other known or projected events in the geological record [27]. Because durable quantum machines may never develop imagination [28], the technology that Joseph Friedlander proposed has formal educational implications for Brazilian Macro-Imagineering/Macro-Engineering because that missing machine skill must then prompt all humans everywhere to markedly cultivate Homo sapiens' generally supposed unique capacities of sensing, understanding, handling, and innovating Earthly and extra-planetary alterations, either intentionally or unintentionally.

3. A mistily conceived Serpa-Cathcart world composition manipulation scheme

Someday Nilo S.C. Serpa's future-realized and multi-planetary bioshell-deployed quantum machine cloud computing model may conveniently enable appropriately trained Homo sapiens representatives to utilize the widely-dispersed on-demand network of nanites postulated by Joseph Friedlander and others since. Although the jargon "cloud computing" has only been widely prevalent since AD 2007, Douglas F. Parkhill's ***The Challenge of the Computer Utility*** (1966) outlined modern-day non-quantum cloud computing's main elements. Certainly, cloud particulates (dust motes, freshwater droplets, ice-crystals, sand grains [29], additive manufacturing industry powder or paste ingredients), which indisputably do have measurable surfaces, are inequivalent to surface-less quantum "points" [30]. But, let us herein project a somewhat vague granular conception that may become useful in a near-term future real-world practical volumetric Brazilian Geography. GEOGRAPHOS takes its stimulus from University of Queensland, Australia, scientists who have created "Schrodinger's Art" — visible images of live persons as well as famous oil and watercolor artist's paintings placed onto normally unseen quantum canvases comprised of Bose-Einstein condensates, https://www.uq.edu/news/article/2019/05/scientists-paint%E2%80%99-mona-lisa-quantum-canvas; their work combines the dexterous skills of artistic cartographers utilizing the "pointillism" style of Georges Seurat (1859-1891) as well as the amateur artist's product manufactured and shop-sold by Dan Robbins (1926-2019) as his commercial popular entertainment, the "paint-by-number" amateur-aimed Art-supply store sold product! Since Earth's innermost core — along with the shell-shaped Earth-mantle — never reached, touched or remotely-directed machine manipulated — is assumed to be an eccentrical, even lumpy, possibly rotating nucleated mass, basically GEOGRAPHOS asserts that the popularized so-called "Anthropocene" is sufficiently best characterized by its anthropogenic *geomer* particulate pollution. Asteroid 2024 YR2 has a ~3% likelihood of hitting Earth in 2032 AD but won't excessive future asteroid mining [31] also cause unlimited particulate pollution if minerals are extracted, shaped for aerodynamic delivery to Earthly customers arrive constantly?

In addition to Brazil's heatwaves and extreme cold weather, particulate matter aerial fallout instigates the greatest human burden of respiratory, cardio-vascular, and neurological illness. Homo sapiens' *Dosmozoicum* Earth-bioshell is most usefully segmented into suitable *geomer* vertical

volumetric units as exposited in its fullest theoretical Geography explanatory detail by Hans Carol (1915-1971) during AD 1961-62 [32]. We might try considering via volumetric thinking the Earth-bioshell as Nature's version of our laboratory "cloud chamber" investigations [33]! Indubitably Nilo S.C. Serpa's careful tentative venture into the geographical realm of "spookytechnology" [34] portends materialization of an unusual shared future biotic/robotic sentient control of the entire Earth-bioshell, with the looming possibility of a control so incontestably complete that it might equal or otherwise surpass the overwhelming active technology possessed by the fictional Krell creatures featured in the 1956 USA-made film ***Forbidden Planet*** [35]. One especially disgusting *Dosmozoicum* techno-social projection: what if government authorities in Brasil as well as worldwide finally modified their real-estate property taxation schemes from a taxpayer-visible basis of measured neutral surface area to a basis of calculated quantum machine network-afforded, and landscape-seascape property titled, three-dimensional *geomer* volume [36]?

For macro-engineers, ground improvement, which increasingly includes underwater sediments, entails modifying the existing physical properties of the ground undergirding the landscape or seascape to enable future effective, economic, and safe construction — that is, to achieve some condition of appropriate macro-engineering performance by densification, consolidation, injections, and in-situ surface mixing through mechanical means of the topmost non-air part of Carol's *geomer*. (The predictability limit, on average, for air's movements and changes, is now just about 15 days and that human or automated skill-set is not expected to improve significantly even with more intense use of the available as well as coming-online quantum machine cloud.) As of AD 2025, the world's smallest sensor is a <0.3 mm cube smaller than a grain of sand and grayish concrete "smart rocks" have long been employed to report on river and canal water flow effects [37]; objects enclosing Radio Frequency Identification chips nowadays pervade volumetrically enormous *geomer* segments of our planet's bioshell including the Earth-atmosphere [38]. An increasing number of in-the-field macro-engineers are carried by autonomous vehicles and oversee drones and robots, some located on offshore mining stations. Mobile material printers — really a manufacturing process contained within a movable machine — are becoming a major technology package present at big geographical-scale 21st Century construction industry worksites worldwide. For hundreds of years humans had to laboriously heft bricks of a limited size simply because of Homo sapiens' somewhat puny physique; that limitation is no longer a real-world necessity due to the presence and operation of drones, AI robots and material printers!

Sadly, in some instances, actual outdoor fieldwork has become unnecessary because of the virtual and augmented realities creatable electronically in any comfortable locale for any purpose! Who today can anticipate what Nilo S.C. Serpa's presciently foreseen spookytechnology will make real for Brazilians and our homeland world's populace? For sure, by cognitive off-loading and other mechanisms or devices, many persons with appropriate technologies are endowed to modify their environment to do some of their thinking for them]. Meantime, more and more frequently, GEOGRAPHOS as well as other individuals and groups have become aware of living, normal persons who became cyborgs — that is, people re-embodied by incorporating unnatural and novel material working technologies after birth into their Nature-induced gene-guided bodies [39]. The Portuguese philosopher Joaquim Pedro Oliveira Martins (1845-1894) remarked at the then astounding mentionable techno-social fact of people's tendencies towards unmonitored individual encapsulation [40]; since then, of course, humans have coped with puffed spacesuits and the tube-shaped degrading supra-structure of the truly dreary, incompletely AI robotized, about to be junked by de-orbit International Space Station.

GEOGRAPHOS envisions our Earth-biosphere will soon take on all the managerial aspects forecast by the stimulating Russian professional geographer Boris Borisovich Rodoman during the 1950s [41]. Whilst studying our immediate planetary environment from the soft matter perspective, we recalled from our long-ago school days Allen Kellogg Philbrick's malleable theoretical Geography innovation,

"…the particulate region" [42]. Philbrick (1914-2007) foresightedly devised an appropriate visualization for all macro-imagineers/macro-engineers, especially those who may have toyed with LEGO units as physiologically-unfettered children! (Grownup micro-engineer David A. Lindon, by 1 August 2024, had fabricated the world's tiniest LEGO piece — only 0.021845 X 0.025170 millimeters—the size of a human white-blood cell.) Data and information about real-world "particulate *geomers*" will be Big Data that seem quite definitely to be fully amenable to Nilo S.C. Serpa's futuristic quantum machines!

4. A new Serpa-Cathcart macro-imagineering archetype

Certainly, Serpa-Cathcart's world composition manipulation scheme includes the visionary perception that AI and quantum computing shall at some point be a forceful part of the macro-imagineering archetype that these authors have built over the past few years. Outside of Big Techs' ideology, non-generative AI can play a relevant role as a predictive support tool in the strategic planning of public policies that meet the growing demand for infrastructure projects, such as the so-called "works of art" in civil engineering (AKA, public works) with macro-engineering dimensions, provided that the core algorithms of machine learning are developed specifically for each demand. Indeed, truly useful AI is that which requires heuristic proficiency in the use of multivariate statistics to create and train efficient neural networks. In a future that is still difficult to pinpoint, the complex processing of large data sets on quantum machines applying gadgets ranging from 100 to 1000 q-bits could serve AI implementations. For now, widespread and everyday quantum computing remains a remote possibility due to the significant challenges ahead. Quantum machines require a high degree of environmental isolation and high thermal control costs in order to deal with the fragility of quantum states while preserving the integrity of the information processed via q-bits. It is assumed that the increased decoherence in q-bits due to device's intrinsic noise can be controlled by advanced machine learning quantum algorithms, but any such claim at the current stage of technology would be premature.

To get an idea of the control difficulties to face, let us remember that quantum states are described by means of a vector orthonormal basis constructed in an abstract Hilbert space [3]. So, let

$$|\epsilon_1\rangle, |\epsilon_2\rangle, |\epsilon_3\rangle, ..., |\epsilon_q\rangle$$

be that orthonormal basis. Thus,

$$\hat{\mathcal{O}}_{\acute{\kappa}} = |\epsilon_{\acute{\kappa}}\rangle\langle\epsilon_{\acute{\kappa}}| \qquad (1)$$

is a quantum intake of information on a screen (a "measurement"), for example. The $\hat{\mathcal{O}}_{\acute{\kappa}}$ forms a set of operators that act upon the Hilbert phase space of the system under macroscopic interaction with $\acute{\kappa}$ possible results of "measurement." The intrinsic intervention of the device modifies the initial state Ψ of the system to

$$\frac{\hat{\mathcal{O}}_{\acute{\kappa}}|\Psi\rangle}{\left(\langle\Psi|\hat{\mathcal{O}}^{\dagger}_{\acute{\kappa}}\hat{\mathcal{O}}_{\acute{\kappa}}|\Psi\rangle\right)^{1/2}} = |\Psi'\rangle; \qquad (2)$$

$$\frac{|\epsilon_{\acute{\kappa}}\rangle\langle\epsilon_{\acute{\kappa}}|\Psi\rangle}{\left(\langle\Psi|\hat{\mathcal{O}}^{\dagger}_{\acute{\kappa}}\hat{\mathcal{O}}_{\acute{\kappa}}|\Psi\rangle\right)^{1/2}} = |\Psi'\rangle; \qquad (3)$$

$$\frac{|\epsilon_{\acute{\kappa}}\rangle\langle\epsilon_{\acute{\kappa}}|\Psi\rangle}{\left(\langle\Psi|\langle\epsilon_{\acute{\kappa}}|\epsilon_{\acute{\kappa}}\rangle|\epsilon_{\acute{\kappa}}\rangle\langle\epsilon_{\acute{\kappa}}|\Psi\rangle\right)^{1/2}} = |\Psi'\rangle; \quad (4)$$

$$\frac{\left|\epsilon_{\acute{\kappa}}\right\rangle\left\langle\epsilon_{\acute{\kappa}}\right|\left.\Psi\right\rangle}{\left(\left\langle\Psi\right|\left.\epsilon_{\acute{\kappa}}\right\rangle\left\langle\epsilon_{\acute{\kappa}}\right|\left.\Psi\right\rangle\right)^{1/2}}=\left|\Psi^{'}\right\rangle; \qquad (5)$$

$$\frac{\left|\epsilon_{\acute{\kappa}}\right\rangle\left\langle\epsilon_{\acute{\kappa}}\right|\left.\Psi\right\rangle}{\left|\left\langle\epsilon_{\acute{\kappa}}\right|\left.\Psi\right\rangle\right|}=\left|\Psi^{'}\right\rangle, \qquad (6)$$

with

$$\left\langle\Psi\right|\left.\Psi\right\rangle=1$$

and

$$\hat{\mathcal{O}}_{\acute{\kappa}}^{\dagger}\hat{\mathcal{O}}_{\acute{\kappa}}=1.$$

Due to that macroscopic intervention of the device, $\epsilon_{\acute{\kappa}}$ shows some classic traces inherited from that device.

However, quantum mechanics says nothing about de world out of the "measurement" — the quantum intake of information on the screen in our case —, and this constitutes a large source of uncertainty. One can imagine the size of the technical obstacle to overcame (even if we think of AI quantum algorithms sufficiently elaborate to minimize decoherence), and we have not even mentioned the possible influences of the environment external to the device.

An important observation to note is that, strictly speaking, we are not convinced of the real gains in processing capacity — considering the technological and environmental costs — of using quantum machines in coordinated large scale instead of classical supercomputers. It seems that it would be more rational to restrict the use of quantum computers, even in clouds, to macro-imagineering projects capable of large physically isolated infrastructures, investing more objectively in classical computers that simulate quantum machines. Indeed, as asserted in [43]: “Geography of the future is therefore…an initiative to cross-fertilize research and epistemologies of the future”. Serpa and Cathcart's new macro-imagineering archetype is inevitable, but it must be thought of in terms of its sustainable applicability if we truly desire a better world.

References

[1] Gabbott, S. and Zalasiewicz (2025) *Discarded: How Technofossils Will be Our Ultimate Legacy.* Oxford University Press) 236 pages.

[2] Lazarus, E.D. and Goldstein, E.B. (2019) Is There a Bulldozer in your Model? *Journal of Geophysical Research: Earth Surface* 124: 696-699.

[3] Serpa, N. (2019) “Prospects on Clouds of Quantum Machines” *CALIBRE: Revista Brasiliense de Engenharia e Fisica Aplicada* 4” 1-25.

[4] Davis, A. (2022) *A World Without Hunger: Josue de Castro and the History of Geography.* (Liverpool, Liverpool University Press) 256 pages.

[5] Simpson, M. (2024) “The Scientific Case Against Net Zero: Falsifying the Greenhous Gas Hypothesis” *Journal of Sustainable Development* 17: 137-157.

[6] Prather, M.J. and Hsu, J.C. (24 September 2019) "A round Earth for climate models" *Proceedings of the National Academy of Sciences* [USA} 116: 19330-19335.

[7] Bothe, O. (13 July 2018) "What even is 'Climate'?" *Geoscience Communication Discussions*. DOI: https://doi.org/10.5194/gc-2018-11 .

[8] Porras, D.C. et al. (2020) "Seeing Gravity: Gait Adaptations to Visual and Physical Inclines—A Virtual Reality Study" *Frontiers in Neuroscience* 13: 1308.

[9] Maus, K.V. et al. (2020) "A global-scale data set of mining areas" *Scientific Data* 7: 289.

[10] Ausubel, J.H. (25 April 1991) "Does climate still matter?" *Nature* 350: 649-652. It has been carefully reported that, in some Earth-bioshell *geomers*, human body temperature has measurably decreased during the 20th Century. Could this remarkable reported metabolic change be somehow related to our commonly experienced air's actual slight warming trend? SEE: Protsive, M et al. (7 January 2020) "Decreasing human body temperature in the United States since the industrial revolution" *eLife* 9: e49555.

[11] Liger-Belair, G. et al. (20 September 2019) "Under-expanded supersonic CO_2 freezing jets during champagne cork popping" *Science Advances* 5: eaav5528.

[12] Melgaco, L. (2017) "Thinking Outside the Bubble of the Global North: Introducing Milton Santos and 'The Active Role of Geography'" *Antipodes* 49: 946-951.

[13] Lastoria, A.C. and Papadimitriou (2012) "Geographical education in Brazil: past and present in 'the country of the future'" *International Research in Geographical and Environmental Education* 21: 327-335.

[14] Alexander, F. et al. (2020) "Exascale applications: skin in the game" *Philosophical Transactions A* 378: 20190056.

[15] Yagian, A.K. et al. (2024) "Metabolic scaling, energy allocation tradeoffs, and the evolution of humans' unique metabolism" *Proceedings of the National Academy of Sciences* 121: e2409674121.

[16] Coimbra, C.F.M. (2025) "Energy Meteorology for the Evaluation of Solar Farm Thermal Impacts on Desert Habitats" *Advances in Atmospheric Sciences* 42: 313-326.

[17] GOTO: https://www.nextbigfuture.com/2015/11/what-if-we-get-ability-to-extract-by_3.html . Joseph Friedlander's posting is dated 30 November 2015.

[18] Teodora, G.S. (9 May 2019) Specialized roots of Velloziaceae weather quartzite rock while mobilizing phosphorus using carboxylates. *Functional Biology* 33, page 76.

[19] Peloggia, A.U.G. (2018) The Rock Cycle of the Anthropocene: Inserting Human Agency into the Earth System. *Revista do Instituto Geologico, Sao Paulo* 39: 1-13.

[20] McNeill (2020) "The volumetric city" *Progress in Human Geography* 44: 815-831.

[21] Torres, P. (March-April 2018) Who would destroy the world? Omnicidal agents and related phenomena. *Aggression and Violent Behavior* 39: 129-138.

[22] Carroll, A.R. (2017) Xenoconformities and the stratigraphic record of paleoenvironmental change. *Geology* 45: 639-642.

[23] Fairen, A.G. (March 2019) The Mars Anthropocene. *Earth & Space Science News* 100: 13-15.

[24] Cathcart, R.B. (2018) *Macro-imagineering our Dosmozoicum*. Mauritius: LAP LAMBERT Academic Publishing.154 pages.

[25] Tilburg, K. Van (2021) "Stellar basins of gravitationally bound particles", *Physics Review D* 104: 023019.

[26] Valero, A., Agudelo, A. and Valero, A. (2011) The crepuscular planet: A model for the exhausted atmosphere and hydrosphere. *Energy* 36: 3745-3753.

[27] Cathcart, R.B. (1983) A Megastructural End to Geologic Time. *Journal of the British Interplanetary Society* 36: 291-297.

[28] Morton, George Ashmun (1903-1983) (February 2000) Machines with Imagination. *Proceedings of the IEEE* 88: 283.

[29] Bridge, G. (2021) "Thinking with the grain" *Dialogues in Human Geography*11: 302-306.

[30] Krause, D. (2019) Does Newtonian Space Provide Identity to Quantum Systems? *Foundations of Science* 24: 197-215.

[31] Dallas, J.A. et al. (2020) "Mining beyond earth for sustainable development: Will humanity benefit from resource extraction in outer space?" *Acta Astronautica* 167: 181-188.

[32] Carol, H. (January 1961) "Geography of the Future". *The Professional Geographer* XIII: 14-18. SEE also: Zur Theorie der Geographie. *Festschrift z. 60, Geburtstag V. Hans Bobek, Mitteilungen der Osterreichischen Gesellschaft* 105:23-38 (1963).

[33] Bertozzi, E. (April 2019) Establishing and Consolidating a Research Field: The Biography of the Wilson Cloud Chamber in the History of Particle Physics. *Historical Studies in the Natural Sciences* 49: 117-150.

[34] Tahan, C. (12 October 2007) Spookytechnology and Society. GOTO: http://arxiv.org/abs/0710.2537. Albert Einstein (1879-1955) neologized the phrase "spooky action at a distance" in "Can Quantum-Mechanical Description of Physical Reality Be Considered Complete?", *Physical Review* 47: 777 (15 May 1935).

[35] Cathcart, R.B. (2017) *Sci-Fi Macro-Imagineering*. West Conshohocken, PA: Infinity Publishing. Chapter One, pages 1-24.

[36] Spankling, J.G. (April 2008) Owning the Center of the Earth. *UCLA Law Review* 55: 979-1040. See also: Wrigley, C. (2023) "Going deep: Excavation, collaboration and imagination at the Kola Superdeep Borehole" *EPD: Society and Space* 4: 549-567. Now, geoscientists are considering the underground as both a resource for various minerals, liquids, and gases but also as a secure place for energy storage and waste deposition. Of course, *geomer* ownership then becomes paramount!

[37] Underwood, E. (14 December 2012) How to Build a Smarter Rock. *Science* 338: 1412-1413.

[38] Frith, J. (2019) *A Billion Little Pieces: RFID and Infrastructures of Identification.* Cambridge: MIT Press. 336 pages.

[39] Preester, H. De (2011) Technology and the Body: the (Im)Possibilities of Re-embodiment. *Foundations of Science* 16: 119-137.

[40] Willdey, C. (Translator) Martins, J.P.O. (1896) *The England of To-Day*. Charing Cross Road, London: George Allen. Page 76.

[41] Cathcart, R.B. (1997) Seeing is Believing: Planetocentric Data Display on a Spherical TV. *Journal of the British Interplanetary Society* 50: 103-104. Also, SEE: Gibney, E. (14 November 2019) "Out of Thin Air" *Nature* 575: 272-273.

[42] Philbrick, A.K. (January 1982) Hierarchical Nodality in Geographic Time-Space. *Economic Geography* 58: 1-19.

[43] Muller-Mahn, D. et al. (2025) "Geographies of the Future" *GEOGRAPHICA HELVETICA*80-177-185. SEE also: Galbrath, E.D. et al. (2025) "Delineating the technosphere: definition, categorization, and characteristics" *Earth System Dynamics* 16:979-999.